Effects of cloud horizontal inhomogeneity and drizzle on remote sensing of cloud droplet effective radius: Case studies based on large-eddy simulations

Zhibo Zhang,[1,2,3] Andrew S. Ackerman,[4] Graham Feingold,[5] Steven Platnick,[3] Robert Pincus,[5,6] and Huiwen Xue[7]

Received 19 February 2012; revised 21 August 2012; accepted 25 August 2012; published 6 October 2012.

[1] This study investigates effects of drizzle and cloud horizontal inhomogeneity on cloud effective radius (r_e) retrievals from the Moderate Resolution Imaging Spectroradiometer (MODIS). In order to identify the relative importance of various factors, we developed a MODIS cloud property retrieval simulator based on the combination of large-eddy simulations (LES) and radiative transfer computations. The case studies based on synthetic LES cloud fields indicate that at high spatial resolution (~100 m) 3-D radiative transfer effects, such as illumination and shadowing, can induce significant differences between retrievals of r_e based on reflectance at 2.1 μm ($r_{e,2.1}$) and 3.7 μm ($r_{e,3.7}$). It is also found that 3-D effects tend to have stronger impact on $r_{e,2.1}$ than $r_{e,3.7}$, leading to positive difference between the two ($\Delta r_{e,3.7-2.1}$) from illumination and negative $\Delta r_{e,3.7-2.1}$ from shadowing. The cancellation of opposing 3-D effects leads to overall reasonable agreement between $r_{e,2.1}$ and $r_{e,3.7}$ at high spatial resolution as far as domain averages are concerned. At resolutions similar to MODIS, however, $r_{e,2.1}$ is systematically larger than $r_{e,3.7}$ when averaged over the LES domain, with the difference exhibiting a threshold-like dependence on both $r_{e,2.1}$ and an index of the sub-pixel variability in reflectance (H_σ), consistent with MODIS observations. In the LES cases studied, drizzle does not strongly impact r_e retrievals at either wavelength. It is also found that opposing 3-D radiative transfer effects partly cancel each other when cloud reflectance is aggregated from high spatial resolution to MODIS resolution, resulting in a weaker net impact of 3-D radiative effects on r_e retrievals. The large difference at MODIS resolution between $r_{e,3.7}$ and $r_{e,2.1}$ for highly inhomogeneous pixels with $H_\sigma > 0.4$ can be largely attributed to what we refer to as the "plane-parallel r_e bias," which is attributable to the impact of sub-pixel level horizontal variability of cloud optical thickness on r_e retrievals and is greater for $r_{e,2.1}$ than $r_{e,3.7}$. These results suggest that there are substantial uncertainties attributable to 3-D radiative effects and plane-parallel r_e bias in the MODIS $r_{e,2.1}$ retrievals for pixels with strong sub-pixel scale variability, and the H_σ index can be used to identify these uncertainties.

Citation: Zhang, Z., A. S. Ackerman, G. Feingold, S. Platnick, R. Pincus, and H. Xue (2012), Effects of cloud horizontal inhomogeneity and drizzle on remote sensing of cloud droplet effective radius: Case studies based on large-eddy simulations, *J. Geophys. Res.*, *117*, D19208, doi:10.1029/2012JD017655.

[1]Physics Department, University of Maryland, Baltimore County, Baltimore, Maryland, USA.
[2]Joint Center for Earth Systems Technology, Baltimore, Maryland, USA.
[3]Laboratory for Atmospheres, NASA Goddard Space Flight Center, Greenbelt, Maryland, USA.
[4]NASA Goddard Institute for Space Studies, New York, New York, USA.
[5]NOAA/Earth System Research Laboratory, Boulder, Colorado, USA.
[6]University of Colorado Boulder, Boulder, Colorado, USA.
[7]Department of Atmospheric and Oceanic Sciences, School of Physics, Peking University, Beijing, China.

Corresponding author: Z. Zhang, Physics Department, University of Maryland, Baltimore County, Baltimore, MD 21250, USA. (zhibo.zhang@umbc.edu)

0148-0227/12/2012JD017655

1. Introduction

[2] Low-level maritime water clouds have a strong cloud radiative forcing [*Hartmann et al.*, 1992] and are thought to be particularly sensitive to aerosol influences owing to their low altitude. A key parameter in aerosol-cloud interactions is the cloud droplet effective radius r_e, which also has a strong influence on cloud radiative effects. In satellite-based retrievals, r_e is most frequently derived together with cloud optical thickness (τ) from reflectance measurements at two wavelengths [*Nakajima and King*, 1990], one usually in the visible or near-infrared spectral region (for example, 0.86 μm), where water has negligible absorption and therefore cloud reflection is determined mainly by τ, and the other in the shortwave infrared (for example, 1.6 μm, 2.1 μm, or 3.7 μm),

where liquid- and ice-phase water have significant absorption and cloud reflectance decreases with increasing r_e. This so-called bi-spectral method has been widely adopted [*Han et al.*, 1994; *Platnick and Twomey*, 1994; *Nakajima and Nakajima*, 1995; *Platnick et al.*, 2003; *Roebeling et al.*, 2006] and forms the basis of global surveys of particle size by the MODIS instruments [*Platnick et al.*, 2003]. Note that in both the operational MODIS cloud product and in this study, τ is defined with respect to the visible spectral region and remains almost invariant from the visible to shortwave infrared regions of interest in this study.

[3] Because of their strong radiative forcing [*Hartmann et al.*, 1992], even small biases in r_e or τ retrievals for low-level maritime water clouds can lead to significant errors in calculations of cloud radiative forcing. It is estimated that even a moderate perturbation to the r_e of these clouds can lead to a global radiative forcing perturbation of around $1\sim2$ W m^{-2} [*Oreopoulos and Platnick*, 2008]. It is therefore critical to identify the sources and magnitudes of bias in the cloud property retrievals for these clouds.

[4] Recently, several studies [*Nakajima et al.*, 2010b; *Seethala and Horváth*, 2010; *Zhang and Platnick*, 2011] have shown that r_e retrievals based on the 3.7 μm MODIS band ($r_{e,3.7}$) are systematically smaller than those based on measurements in the 2.1 μm band ($r_{e,2.1}$). As shown by *Zhang and Platnick* [2011], the difference ($\Delta r_{e,3.7-2.1}$) is strongly dependent on cloud regime: over the trade wind cumulus cloud region, where clouds are often broken, the difference can be as large as 10 μm. These findings indicate substantial uncertainties in the current satellite-based cloud r_e retrievals.

[5] Two hypotheses have been proposed to explain these large differences. One possibility is the presence of drizzle within the cloud. The weighting function for cloud reflectance is a function of the magnitude of absorption [e.g., *Platnick*, 2000; *Zhang et al.*, 2010], such that $r_{e,3.7}$ is weighted more toward cloud top than $r_{e,2.1}$ because of the stronger water absorption and smaller penetration depth of the 3.7 μm band. Drizzle in marine boundary layer clouds causes r_e to increase toward cloud base, a vertical structure that might potentially produce larger values of $r_{e,2.1}$ than $r_{e,3.7}$ [e.g., *Chang and Li*, 2002; *Nakajima et al.*, 2010a, 2010b; *Suzuki et al.*, 2010].

[6] The second hypothesis centers on the role of horizontal inhomogeneity, and possibly three-dimensional radiative transfer effects, in determining cloud reflectance [*Boeke*, 2009; *Hayes et al.*, 2010; *Seethala and Horváth*, 2010; *Zhang and Platnick*, 2011]. Most satellite retrievals, including the bi-spectral method, assume that clouds are both horizontally and vertically homogeneous within the instrument field of view (typically on the order of a few hundred meters to a few kilometers). Unfortunately, this assumption can cause significant errors when the clouds exhibit sizable spatial variability within the sensor field of view [*Marshak et al.*, 2006; *Liang et al.*, 2009; *Di Girolamo et al.*, 2010]. *Zhang and Platnick* [2011] noticed that the $r_{e,3.7}$ and $r_{e,2.1}$ differ most in pixels with both large $r_{e,2.1}$ and large sub-pixel inhomogeneity, and suggested that effects associated with cloud horizontal inhomogeneity may play an important role in causing the observed $\Delta r_{e,3.7-2.1}$ (see section 2 for details).

[7] It must be noted that the two hypotheses should not be considered mutually exclusive as they may both play a role in the observed $\Delta r_{e,3.7-2.1}$. Nevertheless, these hypotheses have very different implications. If $\Delta r_{e,3.7-2.1}$ is a result of drizzle, it could provide useful information, including remote drizzle detection [*Chang and Li*, 2002, 2003; *Kokhanovsky and Rozanov*, 2011]. If $\Delta r_{e,3.7-2.1}$ results from cloud horizontal inhomogeneity, however, it reflects the limitations of the retrieval algorithm assumptions and might be used to assess retrieval quality.

[8] Although an understanding of the relative importance of drizzle and cloud inhomogeneity on MODIS r_e retrievals is desired, it is difficult to separate the influences of these factors using MODIS observations alone. Fortunately, high-resolution cloud resolving models provide a useful tool for cloud remote-sensing studies. A high-resolution cloud resolving model, coupled with a plausible treatment of cloud microphysics, can provide detailed information on cloud macrophysical and microphysical structure. Cloud fields from such a model can be used as input to drive 3-D radiative transfer models to simulate satellite observations. Then, cloud property retrievals based on simulated observations can be compared with the original simulated cloud fields to identify the influence of various factors on passive cloud property retrievals. One of the advantages of such a simulator is its flexibility to accommodate various mechanisms at different levels of complexity. For example, the impact of 3-D effects can be estimated by comparing 3-D with 1-D radiative transfer simulations. The impact of drizzle can be estimated by artificially removing it from the simulated cloud fields. In previous studies, the difference between $r_{e,2.1}$ than $r_{e,3.7}$ has been assessed and analyzed based on MODIS observations and hypotheses have been proposed to explain the difference. In this study, these hypotheses will be tested using synthetic cloud fields from a large-eddy simulation (LES) model. For this purpose, we have developed a MODIS cloud property retrieval simulator using a LES model combined with 1-D and 3-D radiative transfer models. Below we present several case studies based on this simulator and discuss the implications of the results.

[9] The objectives of this study are twofold. First, we will introduce our simulator and demonstrate its capabilities for simulating MODIS cloud property retrievals, including the subtle difference between $r_{e,2.1}$ and $r_{e,3.7}$. Second, using the simulator, we will investigate the effects of cloud horizontal inhomogeneity and drizzle on satellite r_e retrievals based on the bi-spectral method, their relative importance under various circumstances, and the implications for introducing systematic bias in the observational record. In particular, we will attempt to address the following questions: *How and to what extent do drizzle and cloud inhomogeneity affect MODIS $r_{e,2.1}$ retrievals? Do they affect the $r_{e,3.7}$ retrieval in different ways or to different degrees? Finally, can they lead to systematic retrieval bias?*

[10] We will first introduce in section 2 the "plane-parallel r_e bias" using simple idealized cases, as well as summarize recent observational results with respect to differences between MODIS $r_{e,3.7}$ and $r_{e,2.1}$ for maritime water clouds. We will then describe the MODIS simulator in section 3 and the case studies in section 4. Results are discussed in section 5 in the context of MODIS observations.

2. Background

[11] To provide clarity for more detailed discussions below, it is important to briefly introduce the concept of the plane-parallel r_e bias and revisit some 3-D radiative transfer

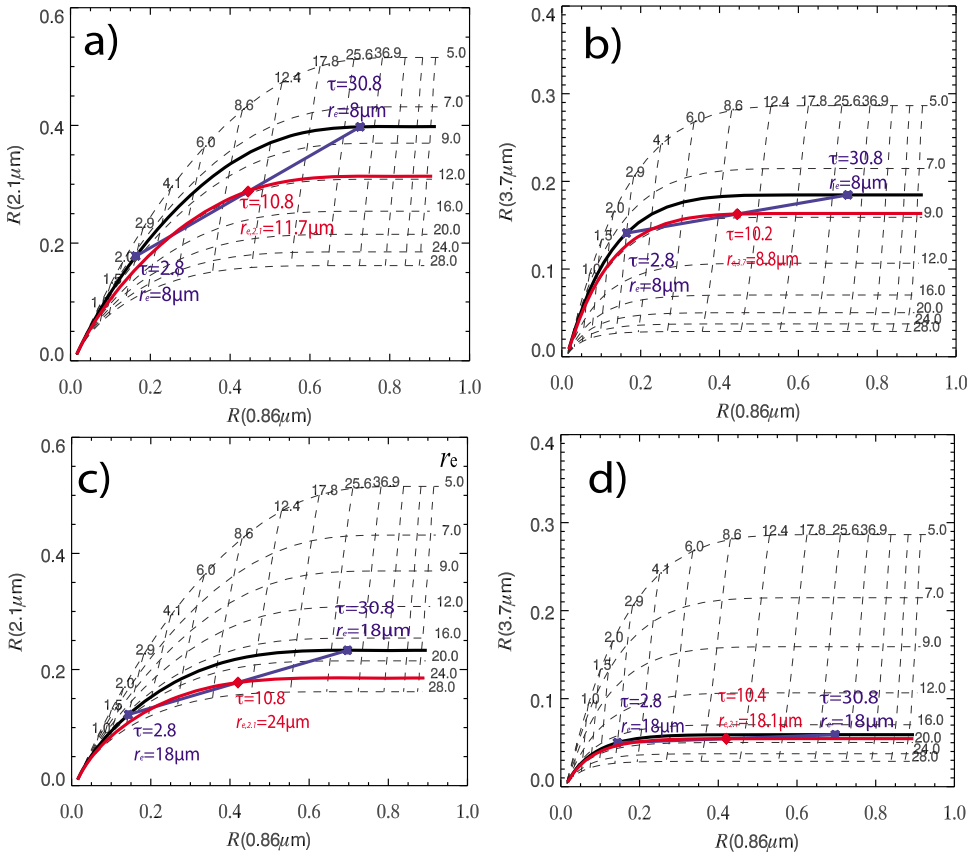

Figure 1. Two theoretical cases to illustrate the nonlinearity effect in r_e retrievals resulting from sub-pixel cloud inhomogeneity. Numbers on top of the Nakajima-King look-up-table (LUT) curves correspond to values of τ contour lines in the LUT, and the numbers on the right of the curves correspond to values of r_e contour lines in the LUT.

effects known to have strong impacts on cloud property retrievals. A summary of the main findings from a recent study of MODIS r_e retrievals for maritime water clouds follows.

2.1. Plane-Parallel r_e Bias

[12] We define the plane-parallel r_e bias as the impact of small-scale variability in τ on r_e retrievals that use area-averaged reflectance. This bias is illustrated using two idealized examples in Figure 1, which shows forward calculations of reflectance in a single non-absorbing band (0.86 μm) and two bands with different amounts of liquid water absorption (2.1 μm and 3.7 μm). In Figures 1a and 1b, we assume that half of a MODIS pixel overlying a black surface is covered by a cloud with $\tau_1 = 2.8$ and $r_e = 8$ μm, and the other half is covered by a cloud with $\tau_2 = 30.8$ and $r_e = 8$ μm. Figures 1c and 1d assume the same optical thickness but use $r_e = 18$ μm. Focusing on the τ retrieval, the figure illustrates the well-known "plane-parallel albedo bias" [*Cahalan et al.*, 1994]: the retrieved τ based on the mean reflectance of inhomogeneous pixels tends to be smaller than the mean of the sub-pixel τ . In this example the value of τ retrieved from the averaged reflectance (10.8) is substantially smaller than the average value (16.8).

[13] This problem is more acute for retrievals of r_e because the reflectance used to infer r_e also depends on τ over much of the range of plausible values. If the reflectance at non-absorbing and absorbing wavelengths depended only on τ and r_e, respectively, (in other words, the look-up-table is orthogonal) reflectance at absorbing wavelengths would be uniform in our example and particle size could be retrieved perfectly. As the figure demonstrates, however, the look-up-table is not orthogonal. The nonlinearity leads to a simultaneous underestimate of τ (i.e., plane-parallel-albedo bias) and overestimate of r_e (i.e., plane-parallel r_e bias). The area over which this is true is larger in the less-absorbing band, which explains why the size overestimate at 2.1 μm is larger than at 3.7 μm (r_e estimates of 11.7 and 8.8 μm, respectively, in Figures 1a and 1b). The impact becomes more pronounced as r_e increases: in Figures 1c and 1d the true r_e = 18 μm while $r_{e,2.1}$ and $r_{e,3.7}$ retrieved from averaged reflectances are 24 μm and 18.1 μm, respectively, resulting in a $\Delta r_{e,3.7-2.1}$ around -6 μm.

[14] It is to be noted that the underlying assumption behind the examples in Figure 1 is that τ has stronger small-scale horizontal variability than r_e. This assumption appears reasonable, as τ can vary over several order of magnitude, while r_e varies mostly from a few to a few tens of microns. On the other hand, if r_e has substantial sub-pixel variability, the configuration of τ and r_e would be different from those in Figure 1. The plausibility of the example shown in Figure 1 will be examined in the LES cases.

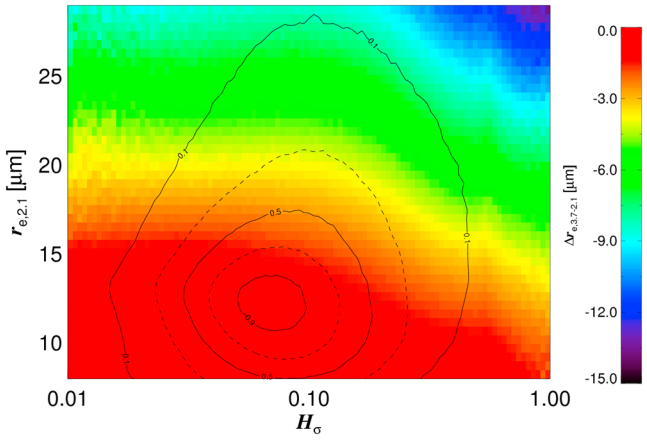

Figure 2. Dependence of $\Delta r_{e,3.7-2.1}$ on cloud effective radius ($r_{e,2.1}$) and cloud horizontal inhomogeneity index (H_σ) derived from one month of operational MODIS observations of warm (cloud top temperature >273 K) liquid-phase clouds over ocean [*Zhang and Platnick*, 2011]. The color shading, with the scale given on the right, corresponds to monthly mean values of $\Delta r_{e,3.7-2.1}$ for clouds with $\tau > 5$ on the space specified by $r_{e,2.1}$ and H_σ. The gray lines indicate the relative frequency of each grid box, specified by selected combinations of $r_{e,2.1}$ and H_σ (unity corresponds to the most frequently observed combination of $r_{e,2.1}$ and H_σ). Thin clouds with $\tau < 5$ are excluded from the figure because of their substantial retrieval uncertainties.

2.2. 3-D Radiative Transfer Effects

[15] Cloud horizontal inhomogeneity can also induce net horizontal transfer of radiation that is neglected by the one-dimensional models on which retrievals are based. Effects of this 3-D radiative transfer, such as illuminating and shadowing, are known to have potential impacts on r_e and τ retrievals [e.g., *Várnai and Davies*, 1999; *Várnai and Marshak*, 2002; *Kato et al.*, 2006; *Marshak et al.*, 2006]. For example, the illuminating effect makes clouds appear brighter than expected under the plane-parallel cloud assumption, resulting in overestimated τ and underestimated r_e retrievals. The shadowing effect makes clouds appear darker, resulting in underestimated τ and overestimated r_e [*Marshak et al.*, 2006].

[16] The 3-D radiative effects may affect $r_{e,2.1}$ and $r_{e,3.7}$ retrievals to different extents and lead to significant differences between the two. In a simple step-cloud case, *Zhang and Platnick* [2011] noted that the 3-D radiative effects tend to have a stronger impact on $r_{e,2.1}$ than $r_{e,3.7}$ (see their Figure 15). This is likely because stronger absorption in 3.7 μm leads to less multiple-scattering and, as a result, less photon horizontal transport. The implication is that the illuminating effect tends to result in positive $\Delta r_{e,3.7-2.1}$ because it reduces $r_{e,2.1}$ more than $r_{e,3.7}$, while the shadowing effect tends to result in negative $\Delta r_{e,3.7-2.1}$ because it increases $r_{e,2.1}$ more than $r_{e,3.7}$.

[17] When a cloud pixel has strong horizontal heterogeneity, both 3-D radiative effects and the plane-parallel r_e bias discussed in the previous section may collude to create either positive or to either positive or negative $\Delta r_{e,3.7-2.1}$. However, because the illuminating and shadowing effects naturally come in pairs and tend to cancel each other [*Marshak et al.*, 2006], the plane-parallel r_e bias might be expected to be the dominant factor when averaged over many cloud cells. We will return to this point in section 5.2.

2.3. MODIS Observations

[18] Many studies have noted that MODIS retrievals of $r_{e,2.1}$ tend to be systematically larger than $r_{e,3.7}$ [*Chang and Li*, 2002; *Nakajima et al.*, 2010b; *Seethala and Horváth*, 2010; *Zinner et al.*, 2010] and that the difference between them, $\Delta r_{e,3.7-2.1}$, is a strong function of cloud regime, varying from 0 to -2 μm over coastal stratocumulus to as large as -5 to -10 μm in regions of broken cumulus [*Zhang and Platnick*, 2011]. *Zhang and Platnick* [2011] demonstrated that underlying the regional dependence was a dependence on the sub-pixel scale variability of non-absorbing reflectance H_σ [*Liang et al.*, 2009]:

$$H_\sigma = \frac{\text{stdev}[R_i(0.86\ \mu\text{m}, 250\,\text{m})]}{\text{mean}[R_i(0.86\ \mu\text{m}, 250\,\text{m})]},$$

where stdev[R_i(0.86 μm, 250 m)] and mean[R_i(0.86 μm, 250 m)] indicate the standard deviation and mean of the measured reflectances, respectively, for the principle sixteen 250 m-resolution sub-pixels within the 1 km MODIS retrieval footprint. Thus, H_σ has a spatial resolution (i.e., 1 km) consistent with the cloud property retrieval and increases with pixel inhomogeneity. The dependence of pixel-level $\Delta r_{e,3.7-2.1}$ on $r_{e,2.1}$ and H_σ in one month of MODIS observations of warm liquid phase clouds (with cloud top temperature >273 K) over ocean is illustrated in Figure 2. The most striking feature is the area of large differences ($\Delta r_{e,3.7-2.1} \sim -10$ μm) in the upper right corner of Figure 2. The large differences are associated with large (>25 μm) values of $r_{e,2.1}$ and large sub-pixel inhomogeneity ($H_\sigma \sim 1$). $\Delta r_{e,3.7-2.1}$ remains stable when H_σ is smaller than about 0.4, but becomes increasingly negative with increasing H_σ when $H_\sigma > 0.4$. For a given H_σ, $\Delta r_{e,3.7-2.1}$ generally increases with $r_{e,2.1}$.

[19] As mentioned earlier, some studies interpret negative values of $\Delta r_{e,3.7-2.1}$ as evidence of drizzle in water clouds, such that the 2.1 μm band (with weak water absorption) penetrates deeper into the cloud than the 3.7 μm band and so can be more strongly affected by large drizzle drops in the lower part of the cloud [*Chang and Li*, 2002; *Nakajima et al.*, 2010a]. Others argue that the difference between $r_{e,2.1}$ and $r_{e,3.7}$ is mainly a result of the plane-parallel r_e bias illustrated in Figure 1. Both hypotheses would find support in Figure 2. The fact that the strongest $\Delta r_{e,3.7-2.1}$ is found where $r_{e,2.1}$ is larger than 25 μm is consistent with the drizzle hypothesis because drizzling clouds tend to have larger r_e than non-drizzling clouds. On the other hand, large values of the sub-pixel inhomogeneity index H_σ in the same region would imply plane-parallel r_e bias in the retrieval.

3. Simulating MODIS Retrievals

[20] Since the two hypotheses cannot be distinguished using the observations alone, we turn to retrievals from synthetic clouds in which the radiative transfer effects can be carefully controlled. Cloud structure is obtained from simulations by the DHARMA LES model [*Stevens et al.*, 2002; *Ackerman et al.*, 2004]. Here, DHARMA uses a single-moment bin microphysics scheme to resolve size distributions of aerosols and activated water drops each into 25 size bins, spanning particle radii of 0.01–2.5 and 1–250 μm, respectively. The size distributions of activated droplets on

Table 1. Summary of Model Setup and Cloud Properties of the Three LES Cases Used for This Study

Case Name	Domain Size	Grid Mesh	Cloud Type	Total Particle Conc. (#/cm^3)	Cloud Coverage[a]	Domain Average τ	Domain Averaged LWP (g/m^2)	Domain Averaged Precipitation Rate at LCL[b] (mm/d)
ATEX Clean	9.6 km × 9.6 km	$\Delta x = \Delta y = 100$ m $\Delta z = 40$ m	Cu	40	72%	5.4	70	0.26
ATEX Polluted	9.6 km × 9.6 km	$\Delta x = \Delta y = 100$ m $\Delta z = 40$ m	Cu	600	78%	8.6	41	0.00
DYCOMS-II (RF02)	6.4 km × 6.4 km	$\Delta x = \Delta y = 50$ m Δz varies	Sc	75[c]	100%	14.5	114	0.07

[a]Cloud coverage is defined as fraction of LES columns with 0.86 μm cloud reflectance larger than 0.02.
[b]Domain-average lifting condensation level (LCL) used as representative of cloud base.
[c]Aerosol size distribution is bimodal for this case; given is the concentration in the accumulation mode.

the DHARMA grid is used to derive cloud scattering properties at MODIS cloud bands, which in turn are used to drive radiative transfer simulations. The bin microphysics approach obviates the requirement of a priori assumptions about cloud drop size distributions. Fields from the LES model described by *Feingold et al.* [1996] and *Xue et al.* [2008] have also been examined, but are not shown here because the results are comparable to our analysis of the DHARMA cases.

[21] Radiative transfer is computed using the I3RC community Monte-Carlo model [*Cahalan et al.*, 2005; *Pincus and Evans*, 2009] for 3-D simulations and the DISORT model [*Stamnes et al.*, 1988] for 1-D simulations. The single-scattering properties of cloud droplets (extinction efficiency $Q_{e,i}$, single-scattering albedo ω_i and phase function P_i) in each size bin, i, are computed using the Mie code of *Wiscombe* [1979], following the steps described by *Platnick and Valero* [1995], for each MODIS band used. In the DISORT model, the scattering properties of a cloudy grid cell are computed off-line by averaging $Q_{e,i}$, ω_i and P_i over the cloud drop size distribution (DSD) from the LES. In the I3RC model, the DSD-averaged scattering properties are constructed online (instead of pre-computed off-line as in the 1-D simulation), from $Q_{e,i}$, ω_i, and P_i based on the cloud DSD. The dynamical construction is implemented through a Monte-Carlo sampling of the relative cumulative extinction function F defined as:

$$F_i = \frac{\sum_{j=1}^{i} Q_{e,j} r_j^2 n_j}{\sum_{j=1}^{N} Q_{e,j} r_j^2 n_j}, i = 1 \ldots N. \quad (1)$$

[22] For a given MODIS band, the shape of F is determined by the cloud DSD. In a scattering event, a random number ζ, uniformly distributed between 0 and 1, is generated. Cloud droplets in the ith size bin with $F_i < \zeta < F_{i+1}$ are then chosen to interact with (i.e., scatter or absorb) the photon. This on-online construction scheme preserves the detail of the cloud microphysical properties from the LES in radiative transfer simulation.

4. Case Studies

4.1. Cloud Fields From Large-Eddy Simulations

[23] Using the MODIS simulator described above, we have investigated the MODIS r_e retrievals for three large-eddy simulations of marine water clouds. The first (referred to as "ATEX clean" hereafter) and second ("ATEX polluted") cases are based on an idealized case study [*Stevens et al.*, 2001] from the Atlantic Trade Wind Experiment (ATEX), with different initial aerosol loadings. A diagnostic approach [*Clark*, 1974] is used for the aerosol, in which the total number concentration of unactivated aerosol particles plus activated droplets is fixed at values of 40 and 600 cm^{-3} for the clean and polluted cases, respectively, resulting in average cloud droplet concentrations (weighted by liquid water mixing ratio) of about 30 and 300 cm^{-3}. The total number and size distribution of activated droplets vary in each grid cell over the course of the simulation. For the 8-h ATEX simulations the domain size is 9.6 km × 9.6 km × 3 km, with a uniform grid mesh of $\Delta x = \Delta y = 100$ m and $\Delta z = 40$ m. (Further details of the model setup for the ATEX cases are provided by *Fridlind and Ackerman* [2011].) A snapshot of the cloud field is taken every half hour over the last 4 h. Therefore, each case contains eight 3-D cloud scenes from the large-eddy simulation, equivalent to about 800 1 km × 1 km pixels. The third case (referred to as the DYCOMS-II case) is based on an idealization of conditions observed during the second research flight (RF02) of the Second Dynamics and Chemistry of Marine Stratocumulus project (DYCOMS-II). For this case, the domain size is 6.4 km × 6.4 km × 1.5 km, and the grid spacing is $\Delta x = \Delta y = 50$ m in the horizontal and stretched vertically, with a spacing minimum of 5 m near the surface and inversion. The average cloud droplet number concentration in the DYCOMS-II case is about 60 cm^{-3}. A snapshot is taken every hour over the last 4 h of the 6-h simulation, yielding about 200 1 km × 1 km pixels. (Further details of the model setup for the DYCOMS-II case are provided by *Ackerman et al.* [2009].) Table 1 provides a summary of model setup and cloud properties for the three cases.

[24] Figure 3 provides a planar view of the cloud τ derived from LES for these three cases. The DYCOMS-II case is almost overcast, while the cloud fraction, defined as fraction of columns with $\tau > 0.1$, in ATEX is around 0.7. Enough drizzle develops in the ATEX clean case that drizzle (i.e., $r >$ 30 μm) accounts for a significant fraction of the total optical thickness τ, but is negligible in the other cloud fields. It is important to note that the cloud τ in Figure 3 is derived from the droplet number concentrations from the LES. It can be different from the τ retrieved from cloud reflectance. The three sets of cloud fields also differ significantly in terms of r_e and cloud inhomogeneity, which we will exploit to help understand the dependence of $\Delta r_{e,3.7-2.1}$ on cloud regimes.

[25] Figure 4 provides an example cloud microphysics simulation from the LES model. The cloud droplet size distributions at three different vertical levels of a selected LES column from the ATEX-clean case are plotted. The location of this column is indicated in Figure 3 (left) by a red star. This particular column is drizzling as indicated by the

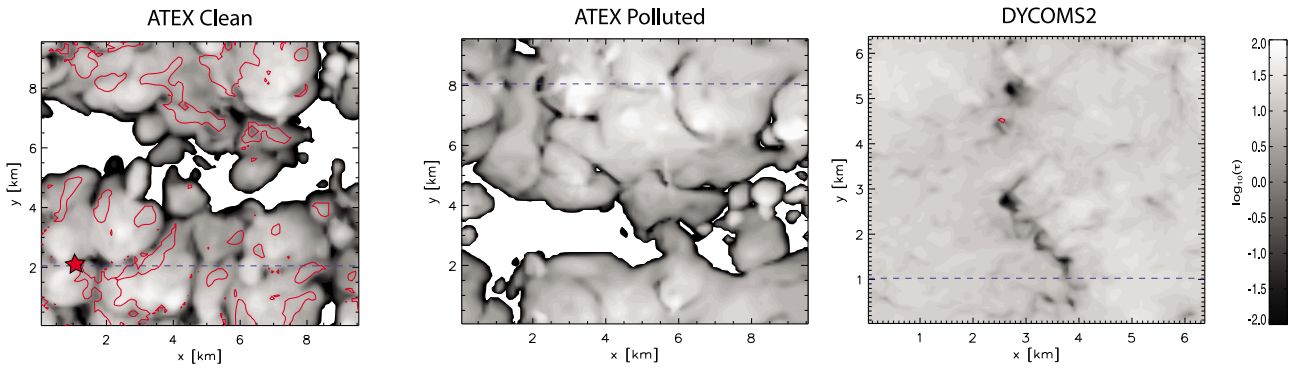

Figure 3. Plan view of the cloud τ of (left) the ATEX clean case at 6 h of simulation time, with the red star indicating the location of the column shown in Figure 4, (middle) the ATEX polluted case at 6 h, and (right) the DYCOMS-II case at 4 h. The red contour indicates where drizzle drops with $r > 30$ μm contribute more than 10% of the cloud τ.

development of the drizzle mode in the size distribution from cloud top toward cloud base. Figure 4 also demonstrates the level of complexity of the LES cloud fields used in this study. In many previous studies based on LES cloud fields, cloud microphysical properties are often greatly simplified. For example, in *Kato et al.* [2006] and *Marshak et al.* [2006] a constant value of r_e is assumed for all cloudy cells. In contrast, in this study every detail of the bin microphysics from the LES model is preserved in the radiative transfer simulations as described in section 3.

4.2. Radiative Transfer Calculations

[26] Both 1-D and 3-D radiative transfer calculations are performed for the 0.86 μm, 2.1 μm and 3.7 μm MODIS bands. Because most of the low-level maritime warm clouds of interest to this study are located in tropical or sub-tropical regions, reflectance is calculated at two solar zenith angles (SZA) (20° and 50°) and a single value of relative azimuth (30°) to simulate the high-sun and low-sun conditions frequently encountered by MODIS over the tropical or subtropical regions [*Seethala and Horváth*, 2010]. Reflectances under each SZA are computed at viewing zenith angles (10° intervals from −50° to 50°) that mimic the scan range of the MODIS instrument. Without explicit indication, retrieval results at different solar and viewing angles are simply combined together in the analysis for more robust statistics; the dependence of results on solar and viewing angles will be investigated later in section 5.2. For simplicity, the surface is assumed to be black and atmospheric absorption is not considered in any of the simulations.

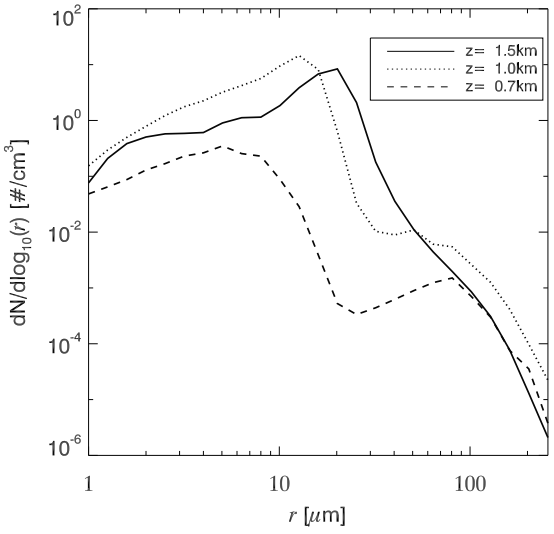

Figure 4. Cloud droplet size distributions at three different vertical levels of a LES column (red star in Figure 3) from the ATEX clean case. The three levels roughly correspond to cloud top (altitude z = 1.5 km), middle of the cloud (z = 1.0 km), and cloud base (z = 0.7 km), respectively.

[27] In practice the 3.7 μm band observation contains both solar reflection and thermal emission components, the latter having to be accounted for during retrieval. We initially included emission in our radiative transfer calculations; however, sensitivity studies (not shown) indicate that including the thermal correction makes no significant difference in the simulation, especially for pixels with $\tau > 5$. For this reason, we will consider only the solar reflection component of the 3.7 μm observation.

[28] We perform retrievals using reflectance at high (native LES) and MODIS-like resolutions; for the latter we use area-averaged reflectance as input to the retrieval. (We have adopted 800 m resolution instead of the nominal 1 km because our model domains are more neatly divisible by 800 m. Sensitivity studies [not shown] indicate the difference between 800 m and 1 km retrievals is negligible.) Given two methods for computing radiative transfer (1-D and 3-D), this produces four sets of retrievals, each of which is affected by different factors (Table 2). High-resolution 1-D

Table 2. Summary of How Different Effects Influence the Retrievals Based on the Different Combinations of Spatial Resolution (LES Native or MODIS) and Radiative Transfer Schemes (1-D or 3-D)

	3-D Radiative Effects	Cloud Vertical Structure and Drizzle Effects	(Plane-Parallel r_e bias)
1-D LES resolution	No	Yes	No
1-D MODIS resolution	No	Yes	Yes
3-D LES resolution	Yes	Yes	No
3-D MODIS resolution	Yes	Yes	Yes

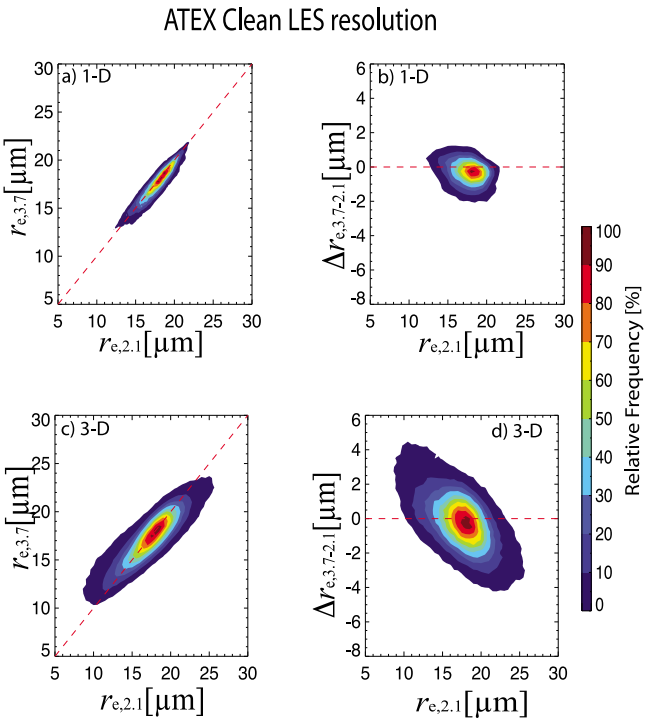

Figure 5. Joint probability distribution of $r_{e,3.7}$ and $r_{e,2.1}$ at the LES resolution for the ATEX clean case: (a) $r_{e,3.7}$ versus $r_{e,2.1}$ based on 1-D radiative transfer simulation, and (b) $\Delta r_{e,3.7-2.1}$ versus $r_{e,2.1}$ from 1-D radiative transfer simulations. (c, d) Same as Figures 5a and 5b but are based on 3-D radiative transfer simulations. Dotted lines indicate 1:1 relation between $r_{e,3.7}$ and $r_{e,2.1}$.

simulations, for example, are free of 3-D radiative effects and plane-parallel r_e bias, but are affected by the cloud vertical structure, including drizzle, so that differences between $r_{e,2.1}$ and $r_{e,3.7}$ retrievals can be attributed to cloud physics. Retrievals simulated at 800 m resolution based on 3-D radiative transfer are affected by all potential factors and resemble real MODIS observations. It is worth pointing out that, no matter which method (i.e., 1-D or 3-D) or resolution (LES native or MODIS) are used in the forward radiative transfer simulations, to be consistent with the operational MODIS product the retrievals are based on the look-up-tables under plane-parallel cloud assumption. A simple threshold method based the cloud reflectance in the 0.86 μm band (i.e., $R(0.86\ \mu m) > 2\%$) is used to mask the cloud pixels after radiative transfer simulation. Only pixels with fractional cloud cover exceeding 0.95 are used in the analysis.

[29] Before proceeding to retrieval results, it is important to point out that although a "reference r_e" is desirable for the comparison between $r_{e,3.7}$ and $r_{e,2.1}$, there are many ways (and therefore *no* unambiguous way) to define a reference r_e from the LES field. To appreciate this, one can consider the LES column in Figure 4. A reference r_e can be defined as $r_e = 3\mathrm{LWP} / (2\tau\rho_w)$, where LWP is the cloud liquid water path of the column and ρ_w is the density of water. Such a reference r_e ensures the correct LWP when τ is known. However, this definition does not account for the fact that the MODIS 2.1 μm and 3.7 μm bands are only sensitive to the upper part of the cloud because of their limited penetration depth [*Platnick*, 2000]. One way to account for this sensitivity is to first derive a vertical weighting function that incorporates both the underlying cloud microphysical structure and the sensitivity of each MODIS band to that structure. Then a reference r_e consistent with the MODIS r_e retrieval mechanism can be derived, based on this weighting function, as described by *Platnick* [2000]. But such a reference r_e is equivalent to the band-specific r_e retrieved from 1-D radiative transfer simulations at LES resolution. Therefore, we simply use the r_e retrieval results from 1-D radiative transfer simulations at LES resolution as the reference r_e.

4.3. Results From the ATEX Clean Case

[30] Figure 5 shows comparisons of $r_{e,2.1}$ and $r_{e,3.7}$ retrievals for the ATEX clean case at the LES resolution based on 1-D (Figures 5a and 5b) and 3-D (Figures 5c and 5d) radiative transfer simulations. To be consistent with the observational results in Figure 2, only those pixels with cloud optical depth $\tau > 5$ are included in Figure 5.

[31] There is relatively little variability in reference r_e in this simulation: most values lie between 13 μm and 22 μm, with very little difference between estimates from 2.1 μm reflectance and those from 3.7 μm reflectance (Figures 5a and 5b). The close agreement between $r_{e,3.7}$ and $r_{e,2.1}$ in Figure 5a suggests that drizzle or cloud vertical structure has either little impact, or affects reflectance at both wavelengths roughly equally. We return to this point in section 5.1.

[32] In 3-D simulations retrieved drop sizes agree well in the range between 15 μm to 20 μm, but $r_{e,3.7}$ overestimates $r_{e,2.1}$ for $r_{e,2.1} < 15$ μm and underestimates $r_{e,2.1}$ for $r_{e,2.1} > 20$ μm. Most reference values of both $r_{e,3.7}$ and $r_{e,2.1}$ are between 15 μm and 20 μm, so these out-of-range retrievals (i.e., $r_{e,2.1} < 15$ and $r_{e,2.1} > 20$ μm) are likely the result of 3-D effects. The results are also consistent with the idea that retrievals in the more-strongly absorbing 3.7 μm band are less affected by 3-D effects than the 2.1 μm band. Under this hypothesis, for example, when 3-D effects lead to an overestimate of true r_e, the overestimate in $r_{e,2.1}$ should be larger than in $r_{e,3.7}$, yielding negative $\Delta r_{e,3.7-2.1}$. This hypothesis will be further explored in section 5.2.

[33] Figure 5 indicates that, though 3-D radiative transfer increases the scatter, retrievals made from reflectance computed at high resolution are broadly consistent across wavelengths. Results at the MODIS resolution, shown in Figure 6, tell a different story: $r_{e,3.7}$ retrievals in both 1-D and 3-D simulations are biased significantly smaller compared with the $r_{e,2.1}$ retrievals. Note also that some very large (>20 μm) $r_{e,2.1}$ retrievals emerge in Figure 6a; $\Delta r_{e,3.7-2.1}$ can be up to -10 μm in these pixels. The 3-D retrieval results in Figures 6c and 6d are quite similar to the 1-D results, suggesting the same mechanism is operative in both 1-D and 3-D retrievals.

[34] Our results are also consistent with the MODIS observations shown in Figure 2. Figure 7 shows composite plots of MODIS resolution $\Delta r_{e,3.7-2.1}$ as a function of $r_{e,2.1}$ and H_σ for both 1-D and 3-D simulations of the ATEX clean case. In the 1-D retrieval (Figure 7a), $r_{e,2.1}$ is mostly between 15 μm and 20 μm and $\Delta r_{e,3.7-2.1}$ remains close to zero until H_σ reaches 0.5, after which $r_{e,2.1}$ rapidly jumps to much larger values and $\Delta r_{e,3.7-2.1}$ drops dramatically from near zero to negative values as large as -10 μm. Consequently, the largest negative values of $\Delta r_{e,3.7-2.1}$ are found at the

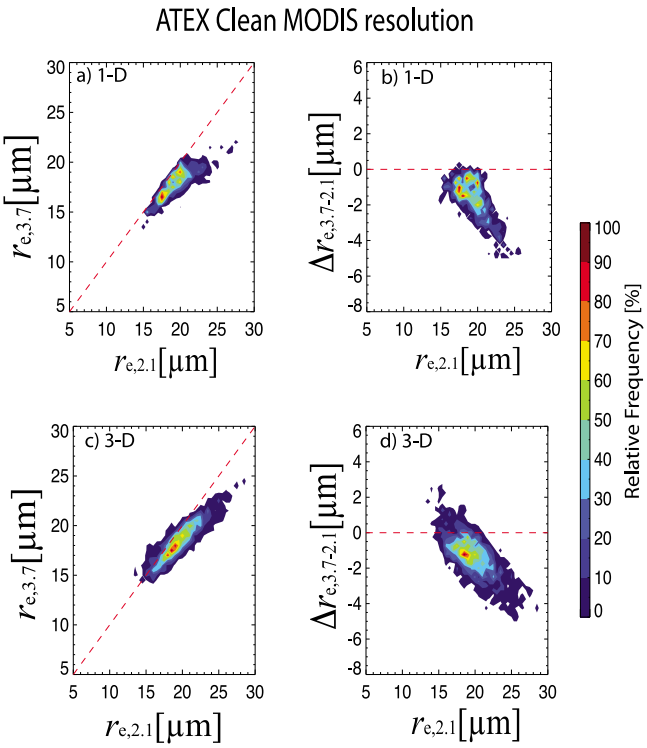

Figure 6. Same as Figure 5 but at MODIS resolution.

upper right corner of Figure 7a, where both $r_{e,2.1}$ and H_σ are large. The 3-D retrievals (Figure 7b) behave much like the 1-D results (Figure 7a), though with more spread and with a less defined threshold. Unique to the 3-D simulations is the transition of $\Delta r_{e,3.7-2.1}$ from red (positive) to green (negative) as $r_{e,2.1}$ increases from 12 μm to more than 20 μm. Positive values of $\Delta r_{e,3.7-2.1}$ correspond to points above the zero line in Figure 6d and above zero in Figure 5d. As discussed above, these points are likely attributable to 3-D radiative effects, such as photon horizontal transport, illuminating and shadowing.

4.4. Results From the ATEX Polluted and DYCOMS-II Cases

[35] Results from the ATEX polluted and the DYCOMS-II cases are consistent with these findings (Figure 8). By design, drop sizes are smaller in the ATEX polluted case (Figures 8a and 8b) than in the ATEX clean examples, with reference r_e values generally below 10 μm. Most pixels in the ATEX polluted case have small-to-moderate $H_\sigma < 0.5$ and stable values of $r_{e,2.1}$ and $\Delta r_{e,3.7-2.1}$, with larger $r_{e,2.1}$ and large negative $\Delta r_{e,3.7-2.1}$ for the small population of pixels with $H_\sigma > 0.5$.

[36] The DYCOMS-II case (Figures 8c and 8d) is almost overcast and the clouds are more homogenous, so that H_σ is small everywhere in the domain and neither the threshold behavior of $r_{e,2.1}$ nor very large negative $\Delta r_{e,3.7-2.1}$ values (i.e., $\Delta r_{e,3.7-2.1} < -5$ μm) are evident. The effects of 3-D radiative transfer are similar to those demonstrated for the ATEX clean case. In particular, 3-D effects have a greater impact on $r_{e,2.1}$ than on $r_{e,3.7}$ so that anomalously small values of $r_{e,2.1}$ (here, less than 14 μm) are associated with positive $\Delta r_{e,3.7-2.1}$, while pixels with abnormally large $r_{e,2.1} > 18$ μm tend to have negative $\Delta r_{e,3.7-2.1}$.

[37] Figures 7 and 8 demonstrate that differences between $r_{e,3.7}$ and $r_{e,2.1}$ retrievals at MODIS resolution in our simulations are largely controlled by the sub-pixel level cloud inhomogeneity: $\Delta r_{e,3.7-2.1}$ becomes increasingly negative as H_σ increases, and the differences are associated with large

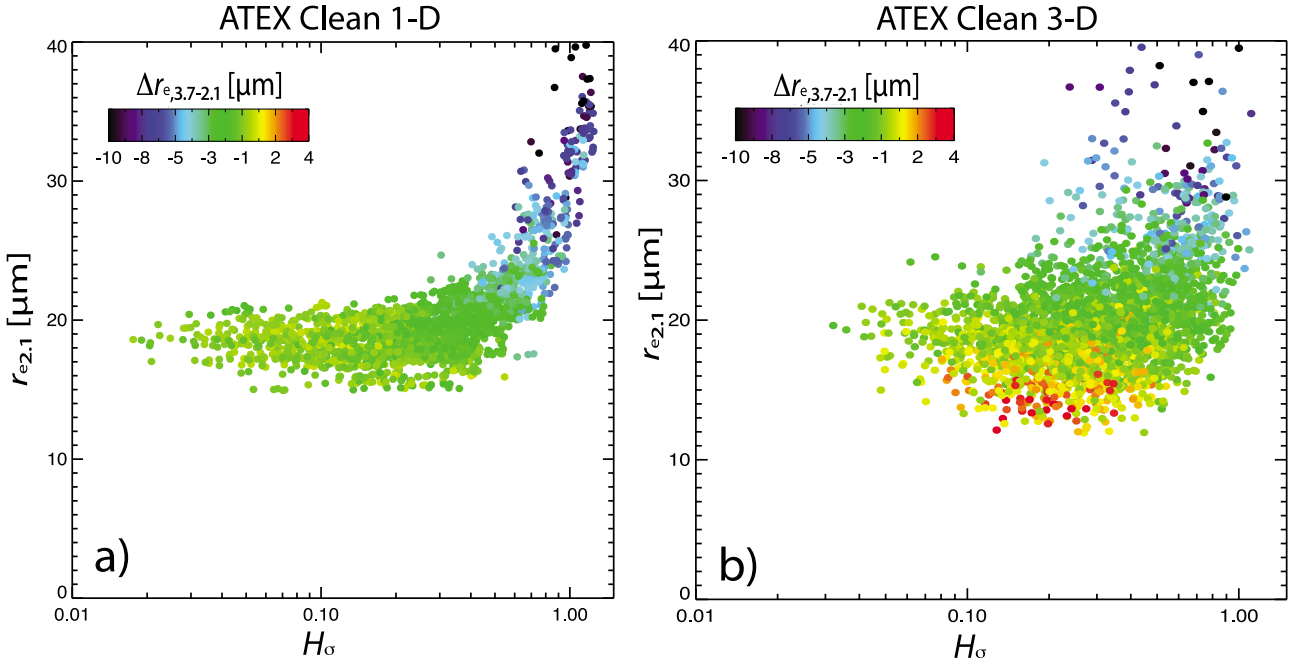

Figure 7. $\Delta r_{e,3.7-2.1}$ at MODIS resolution for the ATEX clean case based on (a) 1-D and (b) 3-D radiative transfer simulations plotted against the sub-pixel inhomogeneity (H_σ) and $r_{e,2.1}$ retrieval. Each dot in the plot indicates a MODIS resolution pixel with color indicating the value of $\Delta r_{e,3.7-2.1}$.

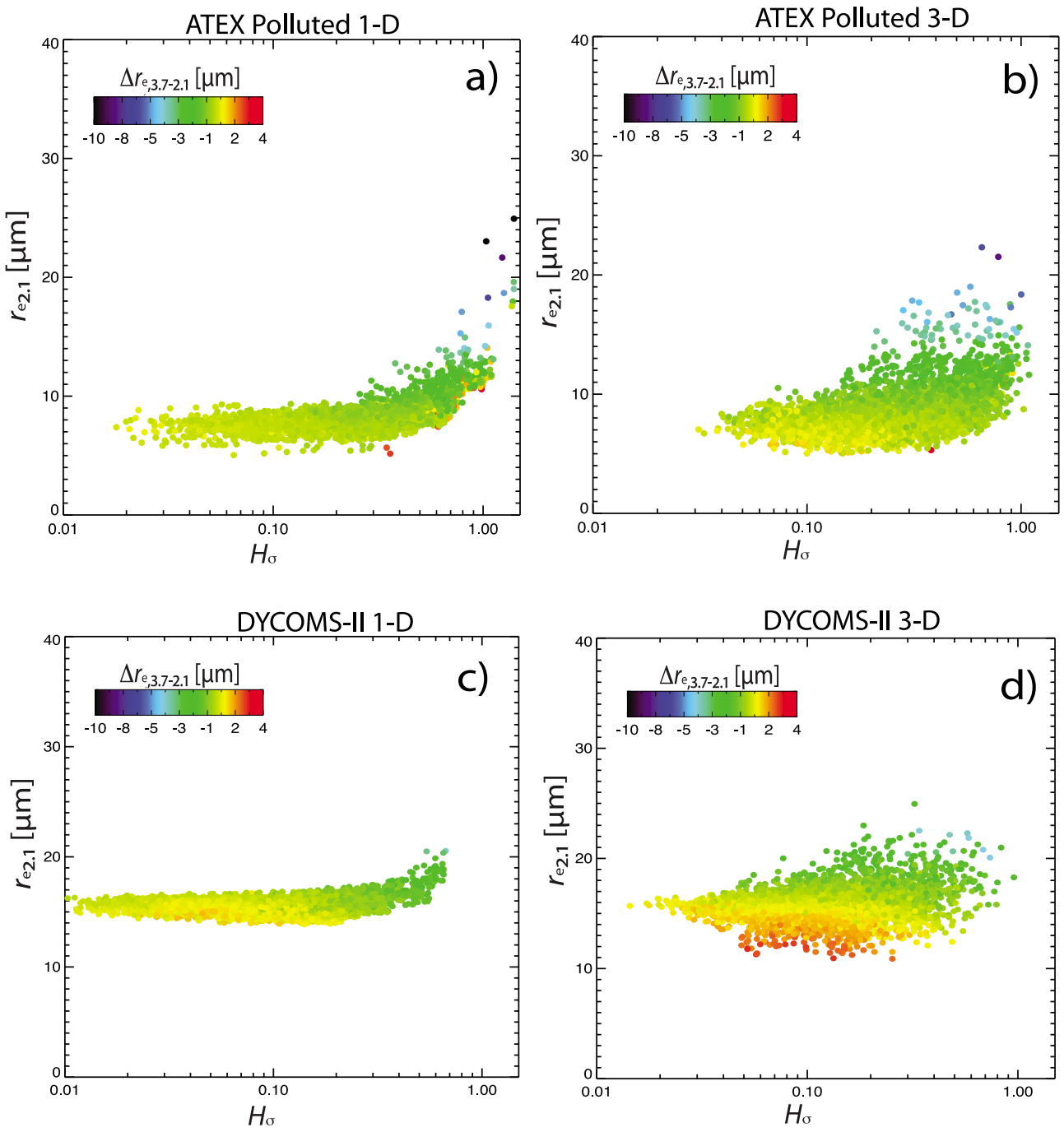

Figure 8. Same as Figure 7 but for (a, b) the ATEX polluted case and (c, d) the DYCOMS-II case.

$H_\sigma \sim 1$, and large $r_{e,2.1}$ retrievals. These results agree well with the MODIS observations shown in Figure 2.

5. Disentangling the Impacts of Drizzle and Cloud Inhomogeneity

[38] In this section we investigate the effect of drizzle and sub-pixel level cloud inhomogeneity on MODIS r_e retrievals, focusing on pixels with the largest magnitude of $\Delta r_{e,3.7-2.1}$ to investigate causal links among $r_{e2.1}$, H_σ and $\Delta r_{e,3.7-2.1}$. We use the ATEX clean case because of its significant drizzle and general consistency with the other two cases.

5.1. Influence of Drizzle

[39] We define drizzle drops as those droplets with $r > 30$ μm, as this threshold generally separates the droplet size distribution into drizzle and cloud modes (see Figure 4). We investigate the impact of these drops on our retrievals by performing calculations in which these drops are removed. Comparisons of LES resolution τ, $r_{e2.1,}$ and $r_{e3.7}$ retrievals based on 3-D reflectances between results that include or

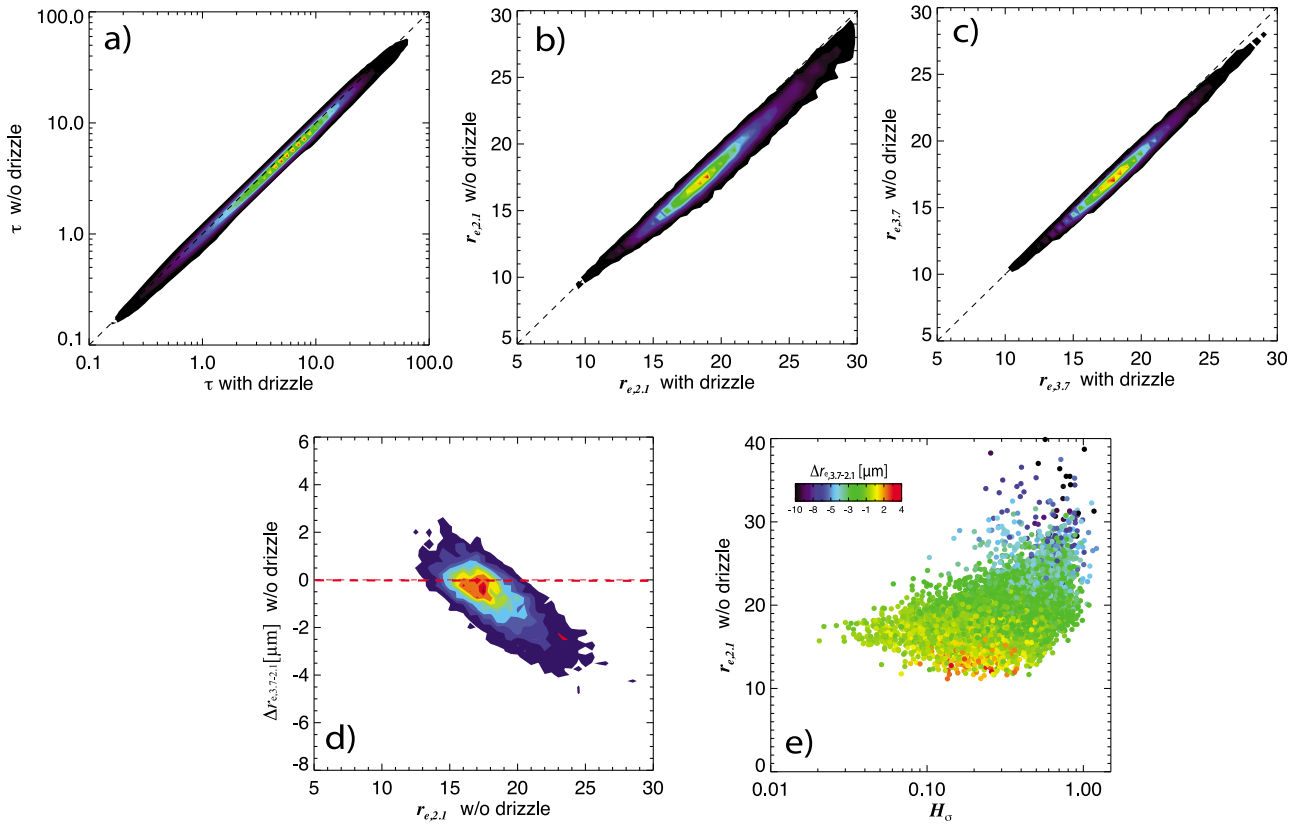

Figure 9. Comparison of (a) τ, (b) $r_{e,2.1}$, and (c) $r_{e,3.7}$ between simulations at MODIS resolution with and without drizzle (defined as drops with radius greater than 30 μm) based on 3-D radiative transfer. (d, e) Same as Figure 6d and Figure 7b, respectively, except that plots in this figure are based on simulations without drizzle.

exclude drizzle drops are shown in Figures 9a, 9b and 9c, respectively. The MODIS resolution retrievals after the removal of drizzle are shown in Figures 9d and 9e in the same manner as in Figures 6d and 7b. The removal of large drizzle drops in the radiative transfer simulation results in slightly smaller cloud optical thickness (Figure 9a) and effective radius retrievals (Figures 9b and 9c), as might be expected, but the differences between simulations with and without drizzle are very small. Indeed, at the MODIS resolution (Figures 9d and 9e), the retrievals after the removal of drizzle look almost identical to those with drizzle (Figures 6d and 7b). Thus drizzle drops with $r > 30$ μm have a very minor impact on the $r_{e2.1}$ and τ retrievals in this particular example, so drizzle cannot be the primary reason for bias between $r_{e,2.1}$ and $r_{e,3.7}$. Similar findings are reported by *Zinner et al.* [2010] and *Painemal and Zuidema* [2011].

[40] We emphasize, however, that the above results are based on a particular LES case, which is not representative of all MODIS observations. For example, a significant fraction of MODIS pixels in Figure 2 have relatively small $H_\sigma \approx 0.1$ and large $\Delta r_{e,3.7-2.1} \approx -5$ μm. However, none of our LES cases yields any retrieval in this region. The impact of drizzle for the pixels in this region therefore remains unclear and needs to be elucidated in future research.

5.2. Influences of Cloud Horizontal Inhomogeneity

[41] We now turn our attention to the plane-parallel r_e bias and 3-D radiative transfer effects. Using the ATEX-clean case we will show that both of these effects exist, and will demonstrate their influence the r_e retrieval. We will then analyze their relative role in causing the $\Delta r_{e,3.7-2.1}$.

[42] The idealized cases in section 2.1 illustrated how cloud horizontal inhomogeneity can result in a plane-parallel r_e bias and significant difference between $r_{e2.1}$ and $r_{e3.7}$. This bias is examined here in a more realistic setting using a pixel from the ATEX clean case. Figure 10 shows the cloud extinction coefficient and cloud reflectance along the cross section at SZA of 20° and viewing zenith angle of 0°. The vertical lines indicate the location of the MODIS resolution pixel analyzed in Figure 11. The 1-D and 3-D simulations of cloud reflectance are in general agreement (i.e., net horizontal transport is small) in all but a few regions in Figure 10b in which $R(0.86$ μm) based on 3-D simulation is substantially smaller than that based on 1-D simulation. The selected MODIS resolution pixel (i.e., 800 m) consists of 64 LES resolution sub-pixels (i.e., 100 m), the reflectances of which are mapped (blue asterisks) onto the retrieval LUTs in Figure 11. The values are clustered around the $r_e = 19$ μm contour line of the LUT. The red diamonds in the figure indicate the locations of the MODIS resolution cloud reflectances, which are simply the linear averages of the blue asterisks. As in the idealized case shown in Figure 1, the MODIS resolution cloud reflectances fall below the envelope of the sub-pixel values in both 1-D (Figures 11a and 11b) and 3-D (Figures 11c and 11d) simulations. As a result, retrievals of $r_{e,2.1}$ at MODIS resolution are around 25 μm, substantially

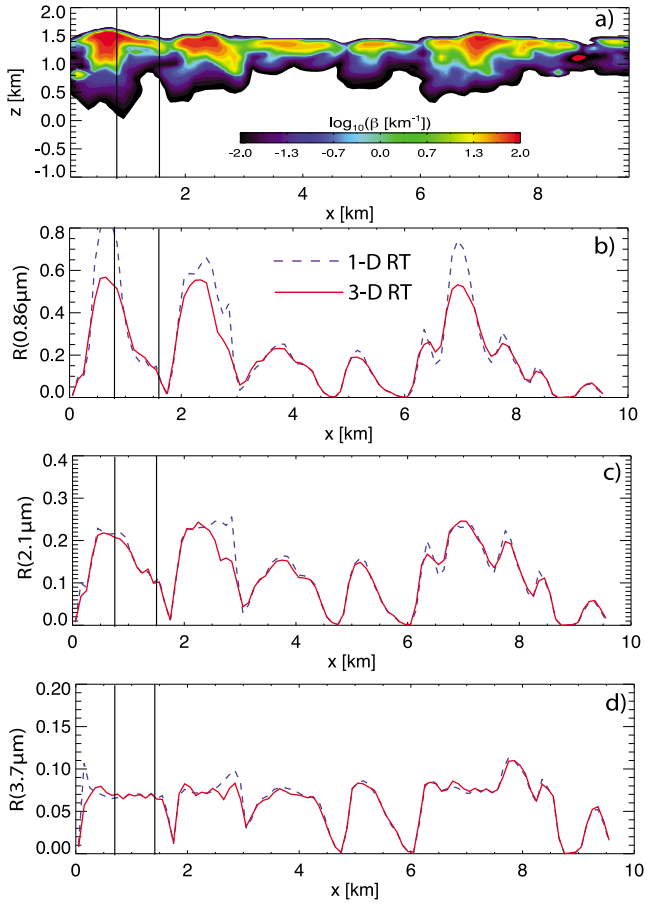

Figure 10. (a) The cross section of cloud extinction coefficient (β) along y = 2 km in Figure 3 (left). Cloud bi-directional reflectance along the cross section is shown for the (b) 0.86 μm, (c) 2.1 μm, and (d) 3.7 μm MODIS bands simulated using 1-D (blue) and 3-D (red) radiative transfer models. The vertical black lines indicate the location of the selected pixel.

larger than the sub-pixel mean value of 19 μm, regardless of whether 1-D (Figure 11a) or 3-D (Figure 11c) radiative transfer is used. Retrievals using 3.7 μm reflectance are less strongly affected: MODIS resolution $r_{e,3.7}$ retrievals (20.5 μm and 21 μm, for 1-D and 3-D radiative transfer simulations, respectively) are much closer to the sub-pixel mean.

[43] The example in Figure 11 shows the existence of plane-parallel r_e bias in our simulation, but is it typical? To investigate this question, we first constructed a sub-pixel variability index for both τ and r_e based on the retrievals from 3-D radiative transfer simulations at LES resolution. The index is defined as the ratio of standard deviation to mean of sub-pixel values. Within the context of Figure 11, a large sub-pixel variability index indicates that the sub-pixel level points are more scattered in the Nakajima-King LUT, whereas small sub-pixel variability index indicates that the sub-pixel level points are clustered around certain constant contour lines of τ or r_e. Figure 12b shows the histograms of the sub-pixel variabilities of τ and r_e for the ATEX-clean case (black line). Evidently, τ has much stronger sub-pixel variability than r_e. This suggests that the example in Figure 11 is a typical case and the r_e heterogeneity factor is an important factor in causing the $\Delta r_{e,3.7-2.1}$. It is worth mentioning that we have also investigated the sub-pixel variability of τ and r_e in real MODIS observation. We developed a research level algorithm to retrieve τ or r_e at 500 m using 500 m radiance observations from the MODIS 0.86 μm and 2.1 μm bands. This algorithm is applied to a MODIS-Terra granule shown in Figure 12a. The sub-pixel variabilities of τ or r_e derived from the 500 m MODIS retrievals (red lines) for this granule are shown in Figure 12b. The good agreement between MODIS observation and LES results confirms that τ tends to vary more strongly than r_e within a 1 km MODIS pixel.

[44] We now turn to the 3-D radiative transfer effects. First, the impacts of 3-D radiative transfer effects on $r_{e,2.1}$ and $r_{e,3.7}$ are investigated in Figure 13. In the figure we use the difference between the τ retrieval based on 3-D radiative transfer simulation (referred to as "3-D τ ") and that based on 1-D radiative transfer simulation (referred to as "1-D τ ") as an index of the 3-D radiative transfer effects. By definition, 3-D τ > 1-D τ for the illuminating effect, and 3-D τ < 1-D τ for shadowing. As expected, the r_e retrievals based on 3-D radiative transfer simulation ("3-D r_e") appear smaller than those based on 1-D radiative transfer simulation ("1-D r_e") for the illuminating effect (i.e., 3-D r_e − 1-D r_e < 0), and vice versa for shadowing (i.e., 3-D r_e − 1-D r_e > 0). What is interesting in Figure 13 is that the impact of 3-D radiative effects on $r_{e,2.1}$ is generally greater than for $r_{e,3.7}$. This is likely attributable to the stronger absorption in the 3.7 μm band that acts to reduce the horizontal transport of photons. The impact of 3-D radiative transfer effects on $\Delta r_{e,3.7-2.1}$ is investigated in Figure 14 as a function of SZA and retrieval resolution. At SZA = 50°, illuminating and shadowing effects are clearly seen in both LES (Figure 14a) and MODIS (Figure 14b) resolution retrievals. Interestingly, based on the 3-D radiative transfer simulations, $\Delta r_{e,3.7-2.1} > 0$ over the illuminated side, and $\Delta r_{e,3.7-2.1} < 0$ over the shadowing side. These are consistent with the result in Figure 13 that illuminating and shadowing effects have stronger impacts on $r_{e,2.1}$ than on $r_{e,3.7}$. For example, over the illuminating side the apparent brightening decreases the r_e retrieval, and this impact is stronger for $r_{e,2.1}$ than $r_{e,3.7}$, leading to positive $\Delta r_{e,3.7-2.1}$. This also explains the origin of the positive $\Delta r_{e,3.7-2.1}$ points in Figures 7 and 8. At SZA = 20°, a significant portion of 3-D τ retrievals are smaller than their 1-D counterparts. This is likely attributable to horizontal photon transport. Unlike illuminating and shadowing effects, which are a result of geometrical cloud top height variation, the horizontal photon transport effect is a result of horizontal τ variation. The absorption in the 2.1 μm and 3.7 μm bands reduces horizontal photon transport, which explains why the absolute values of $\Delta r_{e,3.7-2.1}$ in Figure 14c are generally smaller than those of the low sun case in Figure 14a.

[45] Another interesting point to note in Figure 14 is that, at LES resolution (i.e., Figures 14a and 14c), $\Delta r_{e,3.7-2.1}$ shows no obvious positive or negative bias. However, at MODIS resolution, $\Delta r_{e,3.7-2.1}$ seems biased more toward negative values, which is consistent with the results in Figures 5 and 6. This shift of $\Delta r_{e,3.7-2.1}$ is more clearly seen in Figure 15, which shows $\Delta r_{e,3.7-2.1}$ averaged over all cloudy pixels with $\tau > 5$ in the domain for different solar and

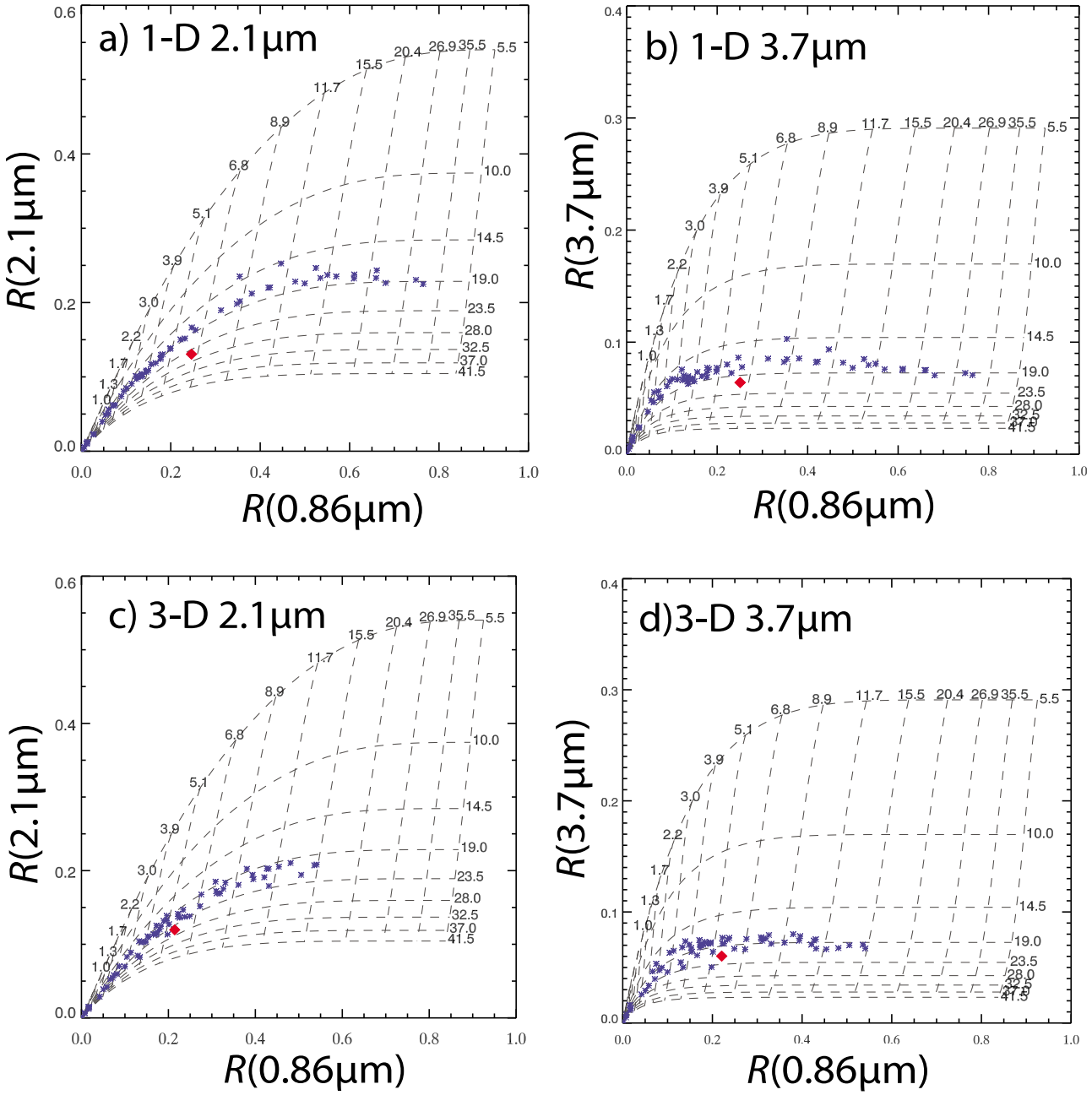

Figure 11. Cloud reflectances of the selected pixel in Figure 10 plotted in the Nakajima-King LUT. The blue asterisks indicate the reflectance simulated at the LES resolution and the red diamond indicates the MODIS resolution radiance calculated as the arithmetic average of the blue dots. The solar and viewing zenith angles for this plot are 20° and 0°, respectively, in this figure.

zenith angles, as well as different retrieval resolutions. In both low sun (SZA = 50°) and high sun (SZA = 20°) simulations, and for all viewing zenith angles, the domain-averaged MODIS resolution $\Delta r_{e,3.7-2.1}$ (red lines) based on 3-D radiative transfer simulations is systematically smaller than its LES resolution counterpart (black lines). This indicates that the shift of $\Delta r_{e,3.7-2.1}$ from close-to-zero values to more negative values when reflectance is averaged from high resolution to MODIS resolution is a robust result, only weakly affected by solar and viewing zenith angles.

[46] The results in Figures 14 and 15 seem to suggest that although the 3-D radiative transfer effect has a strong impact on r_e retrievals, it tends to result in random errors rather than systematic bias. Therefore it is reasonable to hypothesize that the systematic shift of $\Delta r_{e,3.7-2.1}$ seen in Figures 6 and 15 is mainly attributable to the plane-parallel r_e bias. This hypothesis is further investigated in Figures 16 and 17. Figure 16 shows a comparison of the MODIS resolution retrievals with the mean of the LES resolution retrievals (referred to as the sub-pixel mean hereafter). In the case of

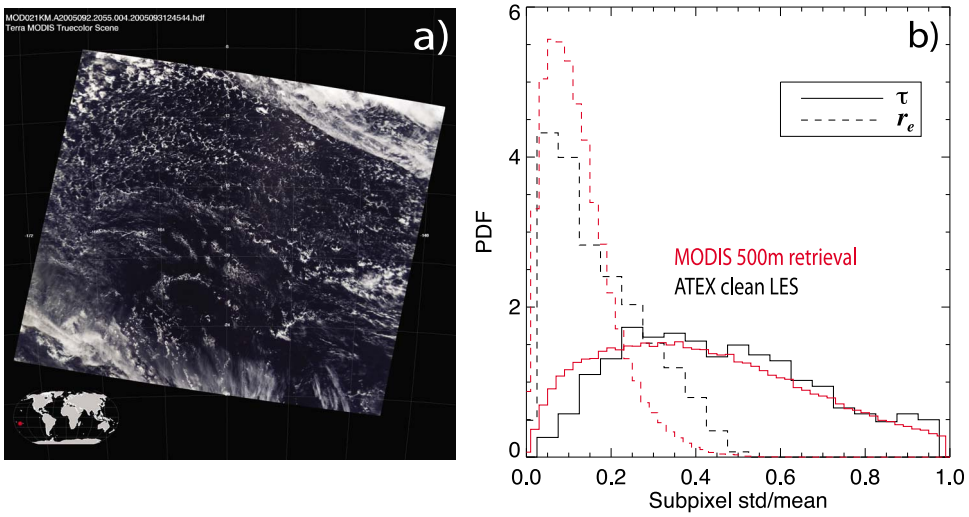

Figure 12. A comparison of sub-pixel variability of τ and r_e between results from MODIS 500 m retrievals and those based on LES. (a) The RGB image of a Terra-MODIS granule (collected at 20:55 UTC on April 2nd, 2005) selected for comparison. A research level algorithm is developed to retrieve τ and r_e from 500 m resolution radiance from MODIS band 2 (0.86 μm) and band 6 (2.1 μm) for this selected granule. Sub-pixel variability of τ and r_e are derived for 1 km resolution operational MODIS pixels (i.e., each 1 km pixel contains four 500 m sub-pixels). (b) The MODIS 500 m retrieval results (red) in comparison with those from the ATEX clean case (black).

the τ retrieval, the plane-parallel bias is evident: values retrieved from the averaged radiances (i.e., MODIS resolution retrieval) are significantly smaller than the sub-pixel mean values. However, in the case of $r_{e,2.1}$ retrievals, the reverse is true: MODIS resolution retrievals tend to be larger than the sub-pixel mean values. This difference indicates that in comparison with other factors, such drizzle and 3-D radiative transfer, the plane-parallel r_e bias is the dominant source of errors in the $r_{e,2.1}$ retrievals at MODIS resolution. The relationship between the plane-parallel r_e bias and $\Delta r_{e,3.7-2.1}$ is shown more clearly in Figure 17. In both 1-D and 3-D simulation, the magnitude of $\Delta r_{e,3.7-2.1}$ is, in general, positively correlated with the strength of the plane-parallel r_e bias because the plane-parallel r_e bias has a stronger impact on the $r_{e,2.1}$ than on $r_{e,3.7}$. As this bias increases, $r_{e,2.1}$ deviates from the sub-pixel mean, while $r_{e,3.7}$ remains relatively close to the sub-pixel mean, thereby resulting in negative and increasing $\Delta r_{e,3.7-2.1}$. Together Figures 16 and 17 support the hypothesis that the plane-parallel r_e bias is the primary reason for the systematic bias in the $r_{e,2.1}$ retrievals, leading to significant $\Delta r_{e,3.7-2.1}$ values. It should be mentioned here that *Marshak et al.* [2006] found that $r_{e,2.1}$ retrievals tend to decrease with increasing horizontal scale, which is opposite to what we found here. The difference between these two studies might be attributable to the use of different LES fields, different levels of complexity in cloud microphysics (a constant r_e = 10 μm for the whole cloud field was used by *Marshak et al.* [2006], while more realistic r_e fields from a bin microphysics scheme are used in this study), or different configurations in radiative transfer simulations.

[47] To summarize the lessons learned from the above case studies, we use the following equation to qualitatively describe the impact of various factors on MODIS r_e retrieval:

$$r_{e,\lambda} = r^*_{e,\lambda} + \Delta r^{3D}_{e,\lambda} + \Delta r^{PP}_{e,\lambda}, \quad (2)$$

where the subscript λ indicates the spectral band (i.e., 2.1 μm or 3.7 μm) used in the retrieval. In this equation, we use the $r^*_{e,\lambda}$ term to denote the "ground truth," the $\Delta r^{3D}_{e,\lambda}$ term to represent the impact of the 3-D radiative effects (i.e., illuminating or shadowing effects) on r_e retrieval and the $\Delta r^{PP}_{e,\lambda}$ term for the plane-parallel r_e bias. First, it is important to note that even the "ground truth" $r^*_{e,\lambda}$ is dependent on the spectral band owing to, for instance, the spectral difference in vertical weighting. Second, our case studies demonstrate that the $\Delta r^{3D}_{e,\lambda}$ and $\Delta r^{PP}_{e,\lambda}$ terms and their relative impact on $r_{e,\lambda}$ depend on both spectral band and spatial resolution. At high resolution (i.e., LES resolution), the $\Delta r^{PP}_{e,\lambda}$ term is small and $\Delta r^{3D}_{e,\lambda}$ term dominates, leading to substantial difference between 1-D and 3-D retrievals (see Figure 13). Note that the sign of $\Delta r^{3D}_{e,\lambda}$ term could be either positive or negative, depending on the nature of the 3-D effect (i.e., illuminating or shadowing). From a spectral perspective, because the 3-D effects tend to impact $r_{e,2.1}$ more than $r_{e,3.7}$, the absolute value of $\Delta r^{3D}_{e,2.1}$ tends to be greater than $\Delta r^{3D}_{e,3.7}$ (see Figure 14). At high resolution the sign of $\Delta r_{e,3.7-2.1}$ could be either positive or negative (see Figure 5). When cloud reflectance is aggregated to MODIS resolution, the cancellation of opposing 3-D effects reduces the absolute value of the $\Delta r^{3D}_{e,\lambda}$ term. At the same time, the $\Delta r^{PP}_{e,\lambda}$ term from the plane-parallel r_e bias becomes significant, especially for heterogeneous pixels. Note that because the sub-pixel scale variability of r_e is significantly smaller than that of τ (see Figure 12), the sign of the $\Delta r^{PP}_{e,\lambda}$ term tends to be positive

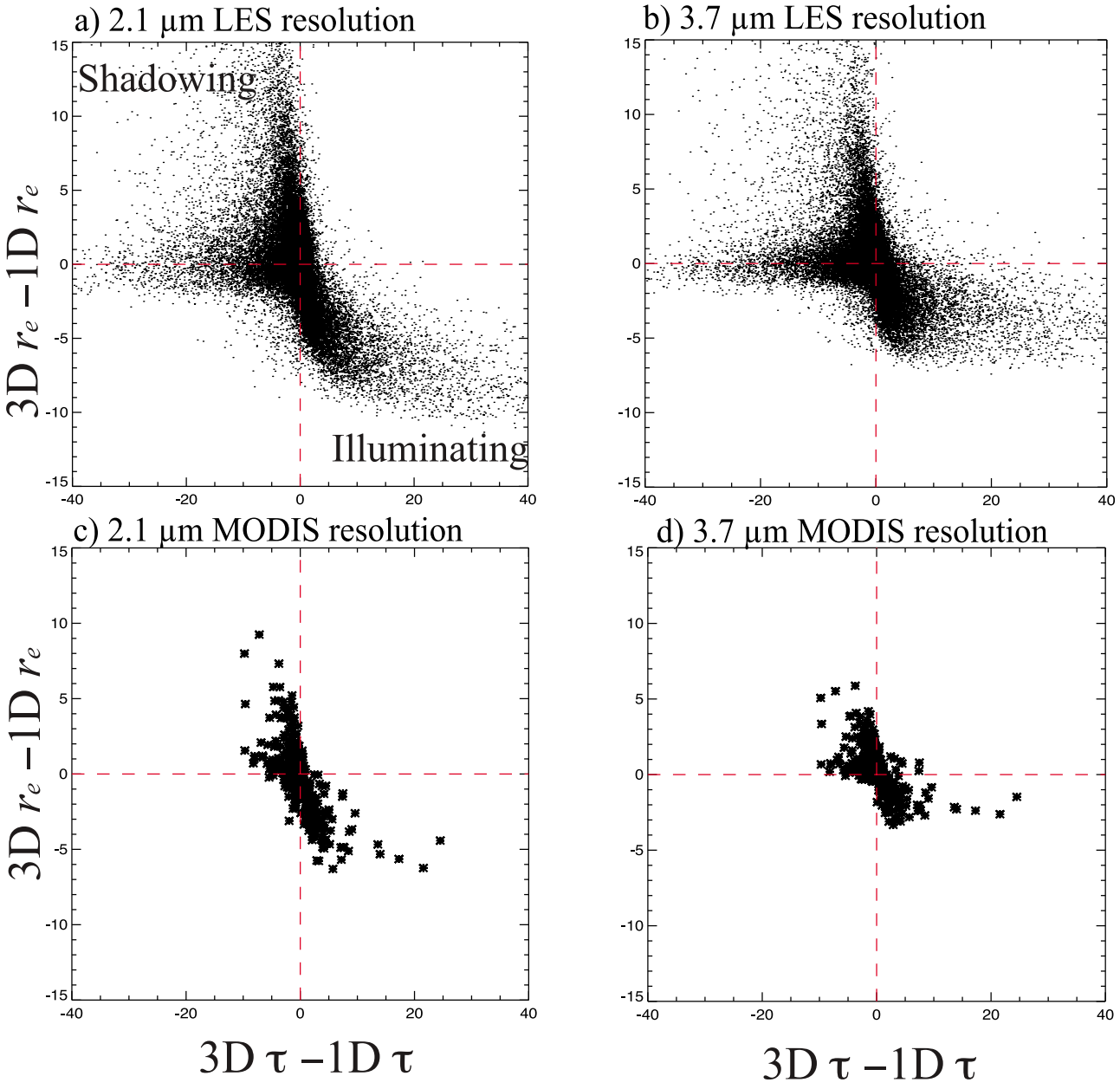

Figure 13. The difference between 3-D and 1-D τ retrieval versus the difference between (a) 3-D $r_{e,2.1}$ and 1-D $r_{e,2.1}$ at LES resolution, (b) 3-D $r_{e,3.7}$ and 1-D $r_{e,3.7}$ at LES resolution, (c) 3-D $r_{e,2.1}$ and 1-D $r_{e,2.1}$ at MODIS resolution, and (d) 3-D $r_{e,3.7}$ and 1-D $r_{e,3.7}$ at MODIS resolution.

(see Figure 1). From a spectral perspective, because the 3.7 μm look-up-table is more orthogonal than 2.1 μm look-up-table, $\Delta r_{e,2.1}^{PP}$ tends to be larger than $\Delta r_{e,3.7}^{PP}$ (see Figures 1 and 11). As a result, at MODIS resolution the $\Delta r_{e,3.7-2.1}$ is biased toward negative values (see Figures 6 and 15) and generally decreases with increasing sub-pixel heterogeneity (see Figure 7), although for individual pixels $\Delta r_{e,3.7-2.1}$ could be either positive or negative depending on the $\Delta r_{e,\lambda}^{3D}$ term. Finally, it should be noted that the $\Delta r_{e,\lambda}^{3D}$ and $\Delta r_{e,\lambda}^{PP}$ terms arise only when a cloud field has significant horizontal heterogeneity. Therefore, these terms cannot explain why some very homogenous pixels in MODIS operational retrievals (i.e., upper-left part of Figure 2) have large negative values of $\Delta r_{e,3.7-2.1}$ (about -5 μm). An explanation for such pixels is left for future studies.

6. Conclusions and Future Work

[48] In this study, we develop a MODIS cloud property retrieval simulator based on the combination of a large-eddy simulation model and radiative transfer models. Using this simulator, MODIS retrievals of shortwave optical depth (τ) and droplet effective radii using 2.1 or 3.7 μm radiances ($r_{e,2.1}$ and $r_{e,3.7}$) are simulated at different resolutions based on both 1-D and 3-D radiative transfer for several LES cases. The effects of drizzle and cloud horizontal inhomogeneity

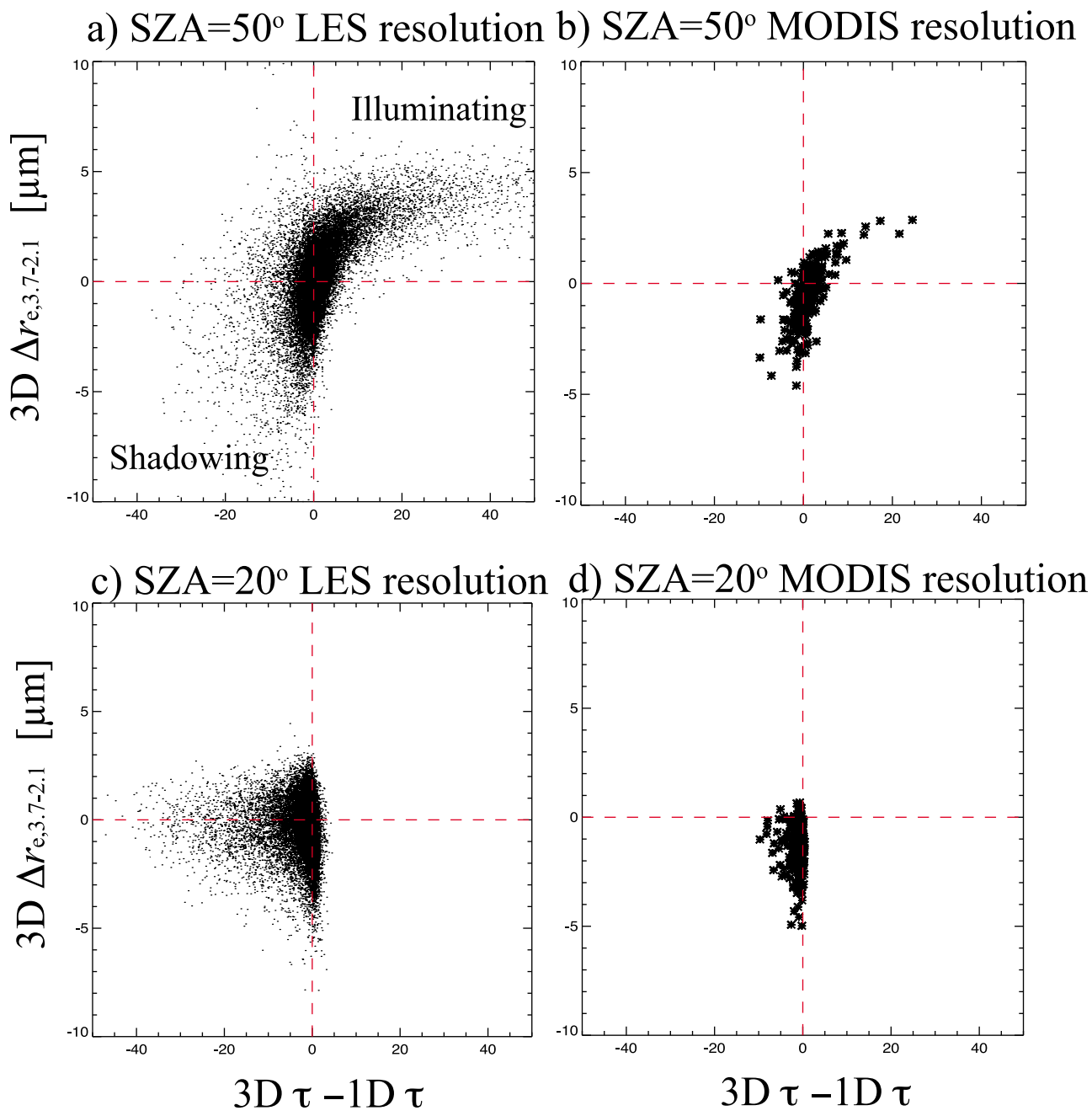

Figure 14. The difference between 3-D and 1-D τ retrieval versus 3-D $\Delta r_{e,3.7-2.1}$ for (a) SZA = 50° at LES resolution, (b) SZA = 50° at MODIS resolution, (c) SZA = 20° at LES resolution, and (d) SZA = 20° at MODIS resolution, based on the retrievals at nadir viewing direction from the ATEX clean case.

on the r_e retrievals in these cases are investigated. It is found that at high resolution (~100 m) 3-D radiative transfer effects, such as enhanced illumination and shadowing, affect $r_{e,2.1}$ stronger than $r_{e,3.7}$ probably attributable to weaker absorption at 2.1 μm. As a result, the illumination effect tends to result in positive $\Delta r_{e,3.7-2.1}$ ($= r_{e,3.7} - r_{e,2.1}$) and the shadowing effect tends to result in negative $\Delta r_{e,3.7-2.1}$. However, because of a balance between these two opposing effects, $r_{e,2.1}$ and $r_{e,3.7}$ agree reasonably well at high resolution, with no systematic bias between the two. At MODIS-like resolution (~800 m), $r_{e,2.1}$ is found to become systematically larger than $r_{e,3.7}$ and the difference is seen to increase with $r_{e,2.1}$ and the sub-pixel inhomogeneity index H_σ, consistent with the trends found in operational MODIS observations. This difference is unlikely a direct radiative result of drizzle here because the removal of drizzle in the radiative computations has little impact on the retrievals, including $\Delta r_{e,3.7-2.1}$. It is also found that opposing 3-D radiative effects tend to cancel each other out at MODIS-like resolution, resulting in a weaker net impact of 3-D effects on r_e retrievals. Finally, it is found within pixels of MODIS-like resolution that cloud τ generally varies more strongly than

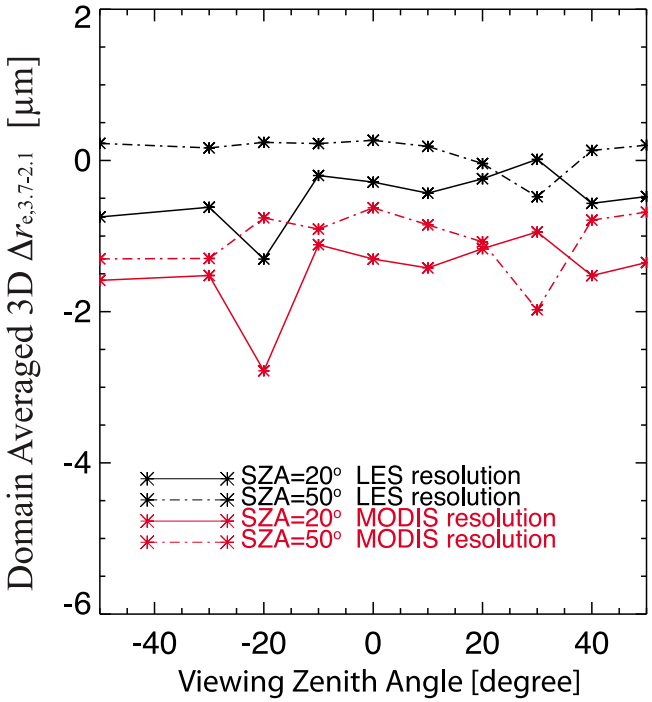

Figure 15. MODIS-resolution $\Delta r_{e,3.7-2.1}$ averaged over all cloudy pixels with $\tau > 5$ based on 3-D radiative transfer simulation for the ATEX clean case at different solar and viewing angles and different retrieval resolutions.

r_e. The strong sub-pixel variability in τ gives rise to an plane-parallel r_e bias that results from averaging over non-orthogonal r_e and τ retrieval curves in the 2-channel (visible and SWIR) radiance phase space, and this heterogeneity bias is largely responsible for the systematic difference between $r_{e,3.7}$ and $r_{e,2.1}$ at MODIS-like resolution

[49] Our results have several implications. First, it is evident from the our analysis, as well as previous studies [*Boeke*, 2009; *Hayes et al.*, 2010; *Seethala and Horváth*, 2010; *Zhang and Platnick*, 2011], that the cloud horizontal inhomogeneity effect can cause substantial errors in MODIS $r_{e,2.1}$ retrievals. The MODIS r_e retrieval based on the 1.6 μm band ($r_{e,1.6}$) is not considered in this study but, given that water absorption is even weaker in this band, we expect that the $r_{e,1.6}$ retrieval faces the same problem. Further investigations are needed to understand the temporal and geographical distributions of this error in the MODIS cloud product, and its implications for climate and aerosol indirect effect studies. Second, it is shown that the inhomogeneity index H_σ can be used to assess the magnitude of such errors, and therefore the quality of MODIS operational $r_{e,2.1}$ retrievals. In fact, in the upcoming MODIS Collection 6 (C6) cloud product, it has been planned for the index H_σ to be reported as part of the cloud mask product (MOD35). Finally, the large negative $\Delta r_{e,3.7-2.1}$ values associated with large H_σ index (i.e., points in the upper right corner of Figure 2) are likely the result of the cloud inhomogeneity effect. This finding warrants caution for the use of these retrievals in cloud vertical structure or drizzle detection algorithms based on $\Delta r_{e,3.7-2.1}$ [*Chang and Li*, 2002, 2003; *Kokhanovsky and Rozanov*, 2011].

[50] Several questions also arise from this study that are worthy of further investigation. For instance, is it possible to reduce the impact of cloud inhomogeneity on the $r_{e,2.1}$ retrieval? Note that the MODIS 2.1 μm band has the native resolution of 500 m. For the limited cases in this study, $r_{e,3.7}$ and $r_{e,2.1}$ agree better at higher resolution. Therefore, it is worth exploring whether the magnitude of $\Delta r_{e,3.7-2.1}$ is substantially reduced if retrievals are made at 500 m resolution. Such investigations would also provide useful information for other satellite instruments, for instance the VIIRS (Visible/Infrared Imager Radiometer Suite) on the Suomi NPP (National Polar-orbiting Partnership) mission, which has a resolution of about 375 m. Another intriguing question is whether $\Delta r_{e,3.7-2.1}$ contains any useful information for cloud vertical structure retrieval or drizzle detection. Note that a significant portion of the large negative $\Delta r_{e,3.7-2.1}$ values are found to be associated with small H_σ index in the MODIS observations (i.e., the pixels in the upper left of Figure 2). Such situations are not represented in our simulation cases. It seems that the cloud inhomogeneity effect is small for such pixels. It remains unclear and warrants further investigation whether these large negative $\Delta r_{e,3.7-2.1}$ values associated with small H_σ reflect the cloud vertical structure [*Chang and Li*, 2002, 2003; *Kokhanovsky and Rozanov*, 2011] or other factors. Finally, future work is also needed to study the impact of cloud horizontal inhomogeneity on ice cloud microphysics retrievals and on other remote sensing techniques, for example the infrared split window method [*Inoue*, 1985; *Prabhakara et al.*, 1988].

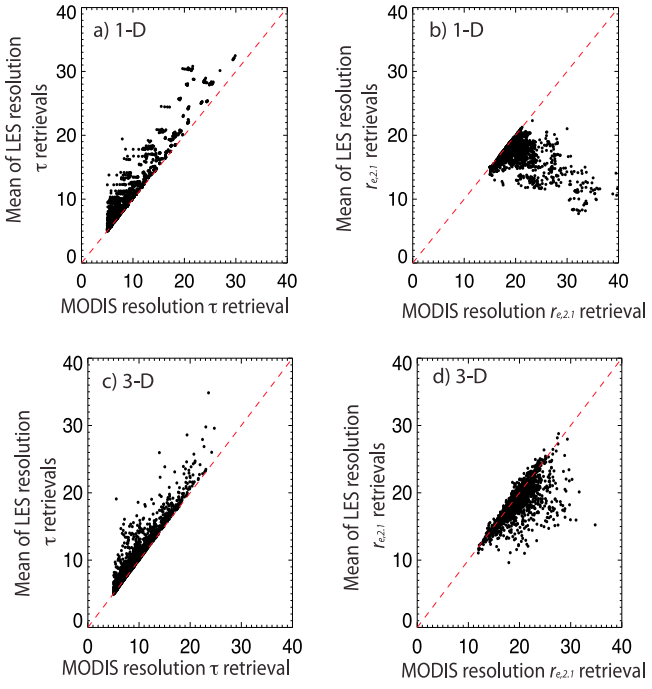

Figure 16. Comparisons between mean retrieval values at LES resolution (i.e., 100 m) with MODIS-like resolution retrievals (i.e., 800 m) based on averaged radiance for (a) τ and (b) $r_{e2.1}$ using the 1-D radiative transfer simulation. (c, d) Same as Figure 16a and Figure 16b, respectively, but are based on 3-D radiative transfer simulations.

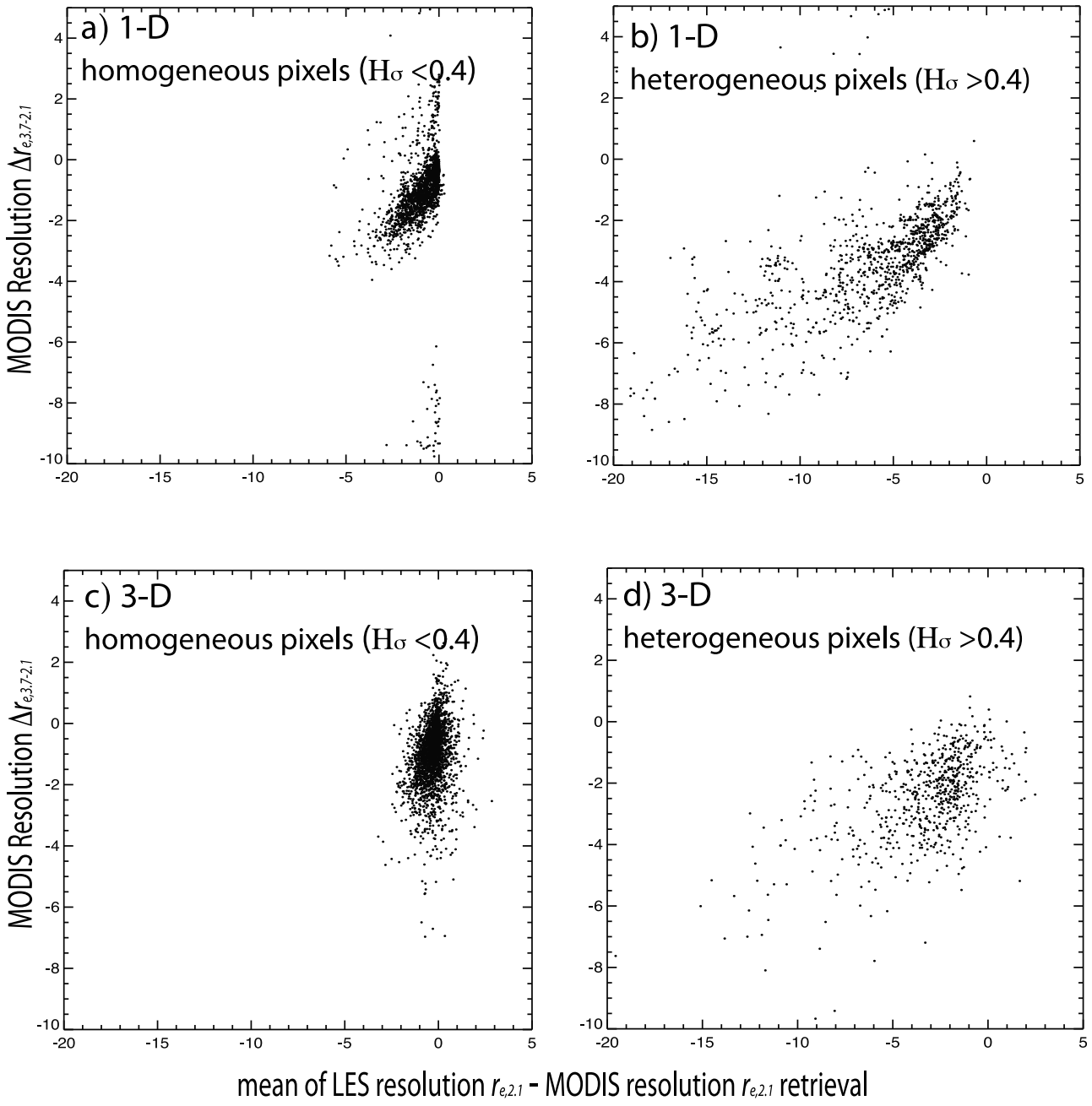

Figure 17. The x axis corresponds to the difference between the sub-pixel means of $r_{e2.1}$ and the $r_{e2.1}$ retrievals at MODIS resolution. The y axis corresponds to the difference $\Delta r_{e,3.7-2.1}$ at the MODIS resolution. The figure shows that $r_{e2.1}$ heterogeneity bias is correlated with $\Delta r_{e,3.7-2.1}$.

[51] **Acknowledgments.** We thank Daniel Grosvenor and the other two anonymous reviewers for their insightful comments, questions, and suggestions, which have helped to improve this manuscript. ZZ, AA and SP were supported by NASA under grant NNX11AI98G, and RP was supported by NASA under grant NNX11AF09G. Computational support was provided by the NASA Advanced Supercomputing Division.

References

Ackerman, A. S., M. P. Kirkpatrick, D. E. Stevens, and O. B. Toon (2004), The impact of humidity above stratiform clouds on indirect aerosol climate forcing, *Nature*, *432*(7020), 1014–1017, doi:10.1038/nature03174.

Ackerman, A. S., M. C. Vanzanten, B. Stevens, V. Savic-Jovcic, C. S. Bretherton, A. Chlond, J. C. Golaz, H. Jiang, M. Khairoutdinov, and S. K. Krueger (2009), Large-eddy simulations of a drizzling, stratocumulus-topped marine boundary layer, *Mon. Weather Rev.*, *137*(3), 1083–1110, doi:10.1175/2008MWR2582.1.

Boeke, R. C. (2009), *Biases in Droplet Radii and Optical Depths of Marine Stratocumulus Retrieved From MODIS Imagery*, Ore. State Univ., Corvallis.

Cahalan, R. F., W. Ridgway, W. J. Wiscombe, T. L. Bell, and J. B. Snider (1994), The albedo of fractal stratocumulus clouds, *J. Atmos. Sci.*, *51*(16), 2434–2455, doi:10.1175/1520-0469(1994)051<2434:TAOFSC>2.0.CO;2.

Cahalan, R. F., et al. (2005), THE I3RC: Bringing together the most advanced radiative transfer tools for cloudy atmospheres, *Bull. Am. Meteorol. Soc.*, *86*(9), 1275–1293, doi:10.1175/BAMS-86-9-1275.

Chang, F. L., and Z. Li (2002), Estimating the vertical variation of cloud droplet effective radius using multispectral near-infrared satellite measurements, *J. Geophys. Res.*, *107*(D15), 4257, doi:10.1029/2001JD000766.

Chang, F. L., and Z. Li (2003), Retrieving vertical profiles of water-cloud droplet effective radius: Algorithm modification and preliminary application, *J. Geophys. Res.*, *108*(D24), 4763, doi:10.1029/2003JD003906.

Clark, T. L. (1974), A study in cloud phase parameterization using the gamma distribution, *J. Atmos. Sci.*, *31*, 142–155, doi:10.1175/1520-0469(1974)031<0142:ASICPP>2.0.CO;2.

Di Girolamo, L., L. Liang, and S. Platnick (2010), A global view of one-dimensional solar radiative transfer through oceanic water clouds, *Geophys. Res. Lett.*, *37*, L18809, doi:10.1029/2010GL044094.

Feingold, G., W. R. Cotton, B. Stevens, and A. S. Frisch (1996), The relationship between drop in-cloud residence time and drizzle production in numerically simulated stratocumulus clouds, *J. Atmos. Sci.*, *53*(8), 1108–1122, doi:10.1175/1520-0469(1996)053<1108:TRBDIC>2.0.CO;2.

Fridlind, A. M., and A. S. Ackerman (2011), Estimating the sensitivity of radiative impacts of shallow, broken marine clouds to boundary layer aerosol size distribution parameter uncertainties for evaluation of satellite retrieval requirements, *J. Atmos. Oceanic Technol.*, *28*(4), 530–538, doi:10.1175/2010JTECHA1520.1.

Han, Q., W. B. Rossow, and A. A. Lacis (1994), Near global survey of effective droplet radii in liquid clouds using ISCCP data, *J. Clim.*, *7*, 465–497, doi:10.1175/1520-0442(1994)007<0465:NGSOED>2.0.CO;2.

Hartmann, D. L., M. E. Ockert-Bell, and M. L. Michelsen (1992), The effect of cloud type on Earth's energy balance: Global analysis, *J. Clim.*, *5*(11), 1281–1304, doi:10.1175/1520-0442(1992)005<1281:TEOCTO>2.0.CO;2.

Hayes, C. R., J. A. Coakley Jr., and W. R. Tahnk (2010), Relationships among properties of marine stratocumulus derived from collocated CALIPSO and MODIS observations, *J. Geophys. Res.*, *115*, D00H17, doi:10.1029/2009JD012046.

Inoue, T. (1985), On the temperature and effective emissivity determination of semi-transparent cirrus clouds by bi-spectral measurements in the 10 micron window region, *Meteorol. Soc. Jpn. J.*, *63*, 88–99.

Kato, S., L. M. Hinkelman, and A. Cheng (2006), Estimate of satellite-derived cloud optical thickness and effective radius errors and their effect on computed domain-averaged irradiances, *J. Geophys. Res.*, *111*, D17201, doi:10.1029/2005JD006668.

Kokhanovsky, A., and V. V. Rozanov (2011), Droplet vertical sizing in warm clouds using passive optical measurements from a satellite, *Atmos. Meas. Tech. Discuss.*, *4*(4), 5597–5629, doi:10.5194/amtd-4-5597-2011.

Liang, L., L. Di Girolamo, and S. Platnick (2009), View-angle consistency in reflectance, optical thickness and spherical albedo of marine water-clouds over the northeastern Pacific through MISR-MODIS fusion, *Geophys. Res. Lett.*, *36*, L09811, doi:10.1029/2008GL037124.

Marshak, A., S. Platnick, T. Várnai, G. Wen, and R. F. Cahalan (2006), Impact of three-dimensional radiative effects on satellite retrievals of cloud droplet sizes, *J. Geophys. Res.*, *111*, D09207, doi:10.1029/2005JD006686.

Nakajima, T., and M. D. King (1990), Determination of the optical thickness and effective particle radius of clouds from reflected solar radiation measurements. Part I: Theory, *J. Atmos. Sci.*, *47*(15), 1878–1893, doi:10.1175/1520-0469(1990)047<1878:DOTOTA>2.0.CO;2.

Nakajima, T. Y., and T. Nakajima (1995), Wide-area determination of cloud microphysical properties from NOAA AVHRR measurements for FIRE and ASTEX regions, *J. Atmos. Sci.*, *52*, 4043–4059, doi:10.1175/1520-0469(1995)052<4043:WADOCM>2.0.CO;2.

Nakajima, T. Y., K. Suzuki, and G. L. Stephens (2010a), Droplet growth in warm water clouds observed by the A-Train. Part I: Sensitivity analysis of the MODIS-derived cloud droplet sizes, *J. Atmos. Sci.*, *67*(6), 1884–1896, doi:10.1175/2009JAS3280.1.

Nakajima, T. Y., K. Suzuki, and G. L. Stephens (2010b), Droplet growth in warm water clouds observed by the A-Train. Part II: A multisensor view, *J. Atmos. Sci.*, *67*(6), 1897–1907, doi:10.1175/2010JAS3276.1.

Oreopoulos, L., and S. Platnick (2008), Radiative susceptibility of cloudy atmospheres to droplet number perturbations: 2. Global analysis from MODIS, *J. Geophys. Res.*, *113*, D14S21, doi:10.1029/2007JD009655.

Painemal, D., and P. Zuidema (2011), Assessment of MODIS cloud effective radius and optical thickness retrievals over the Southeast Pacific with VOCALS-REx in situ measurements, *J. Geophys. Res.*, *116*, D24206, doi:10.1029/2011JD016155.

Pincus, R., and K. F. Evans (2009), Computational cost and accuracy in calculating three-dimensional radiative transfer: Results for new implementations of Monte Carlo and SHDOM, *J. Atmos. Sci.*, *66*(10), 3131–3146, doi:10.1175/2009JAS3137.1.

Platnick, S. (2000), Vertical photon transport in cloud remote sensing problems, *J. Geophys. Res.*, *105*(D18), 22,919–22,935, doi:10.1029/2000JD900333.

Platnick, S., and S. Twomey (1994), Determining the susceptibility of cloud albedo to changes in droplet concentration with the Advanced Very High Resolution Radiometer, *J. Appl. Meteorol.*, *33*(3), 334–347, doi:10.1175/1520-0450(1994)033<0334:DTSOCA>2.0.CO;2.

Platnick, S., and F. P. J. Valero (1995), A validation of a satellite cloud retrieval during ASTEX, *J. Atmos. Sci.*, *52*(16), 2985–3001, doi:10.1175/1520-0469(1995)052<2985:AVOASC>2.0.CO;2.

Platnick, S., M. D. King, S. A. Ackerman, W. P. Menzel, B. A. Baum, J. C. Riedi, and R. A. Frey (2003), The MODIS cloud products: Algorithms and examples from Terra, *IEEE Trans. Geosci. Remote Sens.*, *41*(2), 459–473, doi:10.1109/TGRS.2002.808301.

Prabhakara, C., R. S. Fraser, G. Dalu, M.-L. C. Wu, R. J. Curran, and T. Styles (1988), Thin cirrus clouds: Seasonal distribution over oceans deduced from Nimbus-4 IRIS, *J. Appl. Meteorol.*, *27*(4), 379–399, doi:10.1175/1520-0450(1988)027<0379:TCCSDO>2.0.CO;2.

Roebeling, R. A., A. J. Feijt, and P. Stammes (2006), Cloud property retrievals for climate monitoring: Implications of differences between Spinning Enhanced Visible and Infrared Imager (SEVIRI) on METEOSAT-8 and Advanced Very High Resolution Radiometer (AVHRR) on NOAA-17, *J. Geophys. Res.*, *111*, D20210, doi:10.1029/2005JD006990.

Seethala, C., and Á. Horváth (2010), Global assessment of AMSR-E and MODIS cloud liquid water path retrievals in warm oceanic clouds, *J. Geophys. Res.*, *115*, D13202, doi:10.1029/2009JD012662.

Stamnes, K., S. C. Tsay, K. Jayaweera, and W. Wiscombe (1988), Numerically stable algorithm for discrete-ordinate-method radiative transfer in multiple scattering and emitting layered media, *Appl. Opt.*, *27*(12), 2502–2509, doi:10.1364/AO.27.002502.

Stevens, B., A. S. Ackerman, B. A. Albrecht, A. R. Brown, A. Chlond, J. Cuxart, P. G. Duynkerke, D. C. Lewellen, M. K. Macvean, and R. A. J. Neggers (2001), Simulations of trade wind cumuli under a strong inversion, *J. Atmos. Sci.*, *58*(14), 1870–1891, doi:10.1175/1520-0469(2001)058<1870:SOTWCU>2.0.CO;2.

Stevens, D. E., A. S. Ackerman, and C. S. Bretherton (2002), Effects of domain size and numerical resolution on the simulation of shallow cumulus convection, *J. Atmos. Sci.*, *59*(23), 3285–3301, doi:10.1175/1520-0469(2002)059<3285:EODSAN>2.0.CO;2.

Suzuki, K., T. Y. Nakajima, and G. L. Stephens (2010), Particle growth and drop collection efficiency of warm clouds as inferred from joint CloudSat and MODIS observations, *J. Atmos. Sci.*, *67*(9), 3019–3032, doi:10.1175/2010JAS3463.1.

Várnai, T., and R. Davies (1999), Effects of cloud heterogeneities on shortwave radiation: Comparison of cloud-top variability and internal heterogeneity, *J. Atmos. Sci.*, *56*(24), 4206–4224, doi:10.1175/1520-0469(1999)056<4206:EOCHOS>2.0.CO;2.

Várnai, T., and A. Marshak (2002), Observations of three-dimensional radiative effects that influence MODIS cloud optical thickness retrievals, *J. Atmos. Sci.*, *59*(9), 1607–1618, doi:10.1175/1520-0469(2002)059<1607:OOTDRE>2.0.CO;2.

Wiscombe, W. J. (1979), MIE scattering calculations, advances in technique and fast, vector-shaped computer codes, *NCAR Tech. Note TN-140+STR*, 62 pp. Natl. Cent. for Atmos. Res., Boulder, Colo.

Xue, H., G. Feingold, and B. Stevens (2008), Aerosol effects on clouds, precipitation, and the organization of shallow cumulus convection, *J. Atmos. Sci.*, *65*(2), 392–406, doi:10.1175/2007JAS2428.1.

Zhang, Z., and S. Platnick (2011), An assessment of differences between cloud effective particle radius retrievals for marine water clouds from three MODIS spectral bands, *J. Geophys. Res.*, *116*, D20215, doi:10.1029/2011JD016216.

Zhang, Z., S. Platnick, P. Yang, A. K. Heidinger, and J. M. Comstock (2010), Effects of ice particle size vertical inhomogeneity on the passive remote sensing of ice clouds, *J. Geophys. Res.*, *115*, D17203, doi:10.1029/2010JD013835.

Zinner, T., G. Wind, S. Platnick, and A. S. Ackerman (2010), Testing remote sensing on artificial observations: Impact of drizzle and 3-D cloud structure on effective radius retrievals, *Atmos. Chem. Phys.*, *10*(19), 9535–9549, doi:10.5194/acp-10-9535-2010.